

Concerted Proton–Electron Transfer in the Oxidation of Hydrogen-Bonded Phenols

Ian J. Rhile, Todd F. Markle, Hirotaka Nagao, Antonio G. DiPasquale, Oanh P. Lam, Mark A. Lockwood, Katrina Rotter, and James M. Mayer*

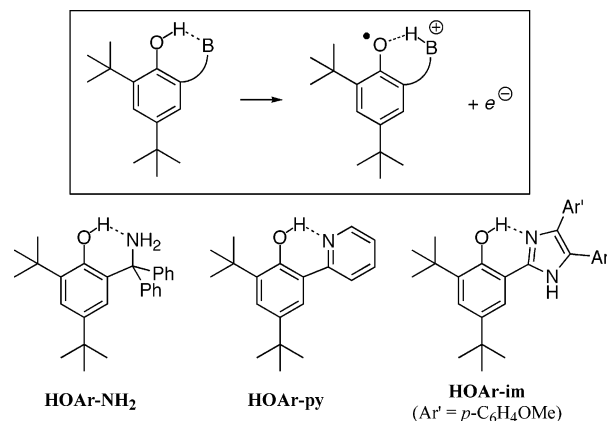
Contribution from the Department of Chemistry, Campus Box 351700, University of Washington, Seattle, Washington 98195-1700

Received June 23, 2005; Revised Manuscript Received March 12, 2006; E-mail: mayer@chem.washington.edu

Abstract: Three phenols with pendant, hydrogen-bonded bases (**HOAr-B**) have been oxidized in MeCN with various one-electron oxidants. The bases are a primary amine ($-\text{CPh}_2\text{NH}_2$), an imidazole, and a pyridine. The product of chemical and quasi-reversible electrochemical oxidations in each case is the phenoxyl radical in which the phenolic proton has transferred to the base, $\bullet\text{OAr-BH}^+$, a proton-coupled electron transfer (PCET) process. The redox potentials for these oxidations are lower than for other phenols, predominately from the driving force for proton movement. One-electron oxidation of the phenols occurs by a concerted proton–electron transfer (CPET) mechanism, based on thermochemical arguments, isotope effects, and $\Delta\Delta G^\ddagger/\Delta\Delta G^\circ$. The data rule out stepwise paths involving initial electron transfer to form the phenol radical cations [$^+\text{HOAr-B}$] or initial proton transfer to give the zwitterions [$^-\text{OAr-BH}^+$]. The rate constant for heterogeneous electron transfer from **HOAr-NH₂** to a platinum electrode has been derived from electrochemical measurements. For oxidations of **HOAr-NH₂**, the dependence of the solution rate constants on driving force, on temperature, and on the nature of the oxidant, and the correspondence between the homogeneous and heterogeneous rate constants, are all consistent with the application of adiabatic Marcus theory. The CPET reorganization energies, $\lambda = 23\text{--}56\text{ kcal mol}^{-1}$, are large in comparison with those for electron transfer reactions of aromatic compounds. The reactions are not highly non-adiabatic, based on minimum values of H_p derived from the temperature dependence of the rate constants. These are among the first detailed analyses of CPET reactions where the proton and electron move to different sites.

Proton-coupled electron transfer (PCET) is of much current interest, as it is important in a variety of chemical and biological processes.^{1,2} Such reactions can occur by concerted or stepwise mechanisms. The stepwise possibilities include initial transfer of the proton followed by electron transfer (PT–ET), sometimes termed proton-gated electron transfer,³ and ET followed by PT (ET–PT). Reactions in which the proton and electron transfers occur in one single kinetic step have recently been termed “concerted proton–electron transfer” (CPET).^{4,5} CPET encompasses a range of processes that involve the transfer of an electron and a proton, including hydrogen atom transfer (HAT),⁶ and non-HAT processes where the e^- and H^+ are separated in the reactants, products, and/or at the transition structure.^{7–11} While HAT reactions continue to be the subject of extensive

Scheme 1



study in organic radical chemistry, the second class of CPET has received less attention. This report describes studies of a set of reactions of the latter class: oxidations of intramolecularly hydrogen-bonded phenols (Scheme 1). Removal of an electron from these compounds results in transfer of the phenolic proton to the base. These reactions involve movement of both e^- and H^+ but cannot be described as HAT.

CPET oxidations of phenols to phenoxyl radicals are of particular importance in biological systems because of the

(1) Cukier, R. I.; Nocera, D. G. *Annu. Rev. Phys. Chem.* **1998**, *49*, 337–369.

(2) Mayer, J. M. *Annu. Rev. Phys. Chem.* **2004**, *55*, 363–390.

(3) For an example, see: Chen, K.; Hirst, J.; Camba, R.; Bonagura, C. A.; Stout, C. D.; Burgess, B. K.; Armstrong, F. A. *Nature* **2000**, *405*, 814–817.

(4) Costentin, C.; Evans, D. H.; Robert, M.; Savéant, J.-M.; Singh, P. S. *J. Am. Chem. Soc.* **2005**, *127*, 12490–12491.

(5) The term PCET has been variously used to refer to all processes involving transfers of H^+ and e^- , specifically only to concerted processes, or to proton-coupled electron transfers that are not HAT. We support the recent suggestion[†] that CPET be used to specifically refer to concerted processes.

(6) (a) *Free Radicals*; Kochi, J. K., Ed.; Wiley: New York, 1973. (b) Mayer, J. M. *Acc. Chem. Res.* **1998**, *31*, 441–450.

(7) (a) Biczók, L.; Gupta, N.; Linschitz, H. *J. Am. Chem. Soc.* **1997**, *119*, 12601. (b) Gupta, N.; Linschitz, H. *J. Am. Chem. Soc.* **1997**, *119*, 6384.

widespread involvement of tyrosyl radicals in enzymatic processes.¹² They have been implicated as intermediates in class I ribonucleotide reductases,¹³ photosystem II,¹⁴ prostaglandin H synthases 1 and 2,¹⁵ cytochrome *c* oxidase,¹⁶ galactose oxidase,¹⁷ amine oxidases,¹⁸ and other systems.¹² In many cases, the phenoxyl radical is generated from the phenol by outer-sphere electron transfer, with release of the proton to a nearby residue (histidine, arginine, lysine, etc.) or to a hydrogen-bonded network.¹² An interesting example is the oxidation of tyrosine 160 of the D₂ subunit (Y_Z) in Photosystem II by long-range electron transfer to the light-induced chlorophyll radical cation P₆₈₀⁺.¹⁹ The phenolic proton of Y_Z is likely transferred to a hydrogen-bonded histidine (His₁₉₀ of subunit D₁). This tyrosyl radical then is involved in the oxidation of the manganese cluster and eventually the conversion of water to O₂.

The **HOAr-B** systems examined here were designed to model such phenol oxidations with concomitant proton transfer. Related model studies include oxidation of tyrosine by a pendant photogenerated [Ru(bpy)₃]³⁺ or a photoexcited Re^I center^{8,9} and electron transfer from phenol–pyridine adducts to photoexcited C₆₀.⁷ These previous studies have all involved intermolecular

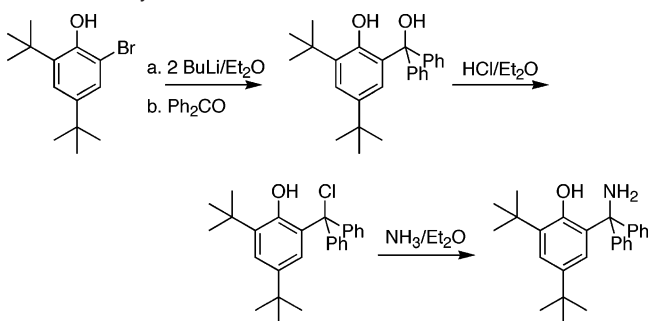
proton transfer (PT), in some cases to bulk solution, while the **HOAr-B** compounds reported here have an intramolecular PT in aprotic media. The use of aprotic media and a strong initial hydrogen bond provides the advantage of being able to keep track of the proton but may limit the generality of the conclusions. More studies are required to model biological and chemical systems with weaker hydrogen-bonding interactions and systems in which the formation of charged intermediates is more facile (perhaps with a higher local effective dielectric constant). Our studies and the model systems mentioned above all conclude that concerted proton–electron transfer is the dominant pathway under most conditions, but Hammarström and co-workers have shown that a proton-first mechanism takes over at high pH, where deprotonation of tyrosine is energetically accessible.⁸ Similarly, elegant work by Okamura and others has indicated stepwise mechanisms for quinone reduction in photosystem I.²⁰

The motif of a tyrosine hydrogen-bonded to a base may be viewed as a biological redox cofactor. A variety of other electron transfer cofactors, such as iron–sulfur clusters, hemes, and quinones, have been studied and understood on the basis of the Marcus–Hush theory of electron transfer.²¹ We have previously shown that rate constants for hydrogen atom transfer reactions are in many cases well predicted by the Marcus cross relation.²² This report shows that Marcus theory can also be applied to non-HAT CPET reactions, and it describes the characteristics of the **HOAr-B** compounds as electron transfer reagents, highlighting the influence of the PT on the thermodynamics and kinetics of electron transfer. The results are also discussed in light of the more recent and more sophisticated theoretical models of CPET.²³ A preliminary report has described the oxidation of one of the phenols, **HOAr-NH₂**.²⁴

Results

1. Syntheses and Characterization of Compounds. The phenol–amine **HOAr-NH₂** was synthesized as outlined in

- (8) (a) Magnuson, A.; Berglund, H.; Korall, P.; Hammarström, L.; Åkermark, B.; Styring, S.; Sun, L. *J. Am. Chem. Soc.* **1997**, *119*, 10720–5. (b) Sjödin, M.; Styring, S.; Åkermark, B.; Sun, L.; Hammarström, L. *J. Am. Chem. Soc.* **2000**, *122*, 3932–3936. (c) Sjödin, M.; Styring, S.; Wolpher, H.; Xu, Y.; Sun, L.; Hammarström, L. *J. Am. Chem. Soc.* **2005**, *127*, 3855–3863. (d) Sjödin, M.; Ghanem, R.; Polivka, T.; Pan, J.; Styring, S.; Sun, L.; Sundström, V.; Hammarström, L. *Phys. Chem. Chem. Phys.* **2004**, *6*, 4851–4858.
- (9) Reece, S. Y.; Nocera, D. G. *J. Am. Chem. Soc.* **2005**, *127*, 9448–9458.
- (10) (a) Shukla, D.; Young, R. H.; Farid, S. *J. Phys. Chem. A* **2004**, *108*, 10386–10394. (b) Turro, C.; Chang, C. K.; Leroi, G. E.; Cukier, R. I.; Nocera, D. G. *J. Am. Chem. Soc.* **1992**, *114*, 4013. (c) Chang, M. C. Y.; Yee, C. S.; Nocera, D. G.; Stubbe, J. *J. Am. Chem. Soc.* **2004**, *126*, 16702–16703. (d) Lehmann, M. W.; Evans, D. H. *J. Phys. Chem. B* **2001**, *105*, 8877–8884. (e) Mayer, J. M.; Hrovat, D.; Thomas, J. L.; Borden, W. T. *J. Am. Chem. Soc.* **2002**, *124*, 11142–11147. (f) Anglada, J. M. *J. Am. Chem. Soc.* **2004**, *126*, 9809–9820. (g) Weatherly, S. C.; Yang, I. V.; Armistead, P. A.; Thorp, H. H. *J. Phys. Chem. B* **2003**, *107*, 372–378. (h) Stubbe, J.; Nocera, D. G.; Yee, C. S.; Chang, M. C. Y. *Chem. Rev.* **2003**, *103*, 2167–2201. (i) DiLabio, G. A.; Ingold, K. U. *J. Am. Chem. Soc.* **2005**, *127*, 6693–6699. (j) Huynh, M. H. V.; Meyer, T. *J. Proc. Natl. Acad. Sci. U.S.A.* **2004**, *101*, 13138–13141. (k) Meyer, T. J.; Huynh, M. H. V. *Inorg. Chem.* **2003**, *42*, 8140–8160.
- (11) (a) Kojima, T.; Sakamoto, T.; Matsuda, Y.; Ohkubo, K.; Fukuzumi, S. *Angew. Chem., Int. Ed.* **2003**, *42*, 4951. (b) Haddox, R. M.; Finklea, H. O. *J. Electroanal. Chem.* **2003**, *550–551*, 351.
- (12) (a) Stubbe, J.; van der Donk, W. A. *Chem. Rev.* **1998**, *98*, 705–762. (b) Pesavento, R. P.; van der Donk, W. A. *Adv. Protein Chem.* **2001**, *58*, 317–385.
- (13) (a) Ehrenberg, A.; Reichard, P. *J. Biol. Chem.* **1972**, *247*, 3485–3488. (b) Sjöberg, B.-M.; Reichard, P.; Gräslund, A.; Ehrenberg, A. *J. Biol. Chem.* **1978**, *253*, 6863–6865. (c) Sahlin, M.; Gräslund, A.; Ehrenberg, A.; Sjöberg, B.-M. *J. Biol. Chem.* **1982**, *257*, 366–369. (d) Gripenburg, U.; Lassmann, G.; Auling, G. *Free Radical Res.* **1996**, *26*, 473–481.
- (14) (a) Barry, B. A.; El-Deeb, M. K.; Sandusky, P. O.; Babcock, G. *J. Biol. Chem.* **1990**, *265*, 20139–20143. (b) Barry, B. A.; Babcock, G. T. *Proc. Natl. Acad. Sci. U.S.A.* **1987**, *84*, 7099–7103.
- (15) (a) Tsai, A.-L.; Kulmacz, R. J.; Palmer, G. *J. Biol. Chem.* **1995**, *270*, 10503–10508. (b) Tsai, A.-L.; Palmer, G.; Kulmacz, R. J. *J. Biol. Chem.* **1992**, *276*, 17753–17759. (c) Tsai, A. L.; Palmer, G.; Xiao, G.; Swinney, D. C.; Kulmacz, R. J. *J. Biol. Chem.* **1998**, *273*, 3888. (d) Hsi, L. C.; Hoganson, C. W.; Babcock, G. T.; Smith, W. L. *Biochem. Biophys. Res. Commun.* **1994**, *202*, 1592–1598.
- (16) (a) Ferguson-Miller, S.; Babcock, G. T. *Chem. Rev.* **1996**, *96*, 2889–2907. (b) Gamelin, D. R.; Randall D. W.; Hay, M. T.; Houser, R. P.; Mulder, T. C.; Canters, G. W.; de Vries, S.; Tolman, W. B.; Lu, Y.; Solomon, E. I. *J. Am. Chem. Soc.* **1998**, *120*, 5246–5263 and references therein. (c) Proshlyakakov, D. A.; Pressler, M. A.; DeMaso, C.; Leykam, J. F.; DeWitt, D. L.; Babcock, G. T. *Science* **2000**, *290*, 1588–1591.
- (17) Whittaker, M. M.; Whittaker, J. W. *J. Biol. Chem.* **1990**, *265*, 9610–9613.
- (18) (a) Janes, S. M.; Mu, D.; Wemmer, D.; Smith, A. J.; Kaur, S.; Maltby, D.; Burlingame, A. L.; Klinman, J. P. *Science* **1990**, *248*, 981–987. (b) Janes, S. M.; Palcic, M. M.; Scaman, C. H.; Smith, A. J.; Brown, D. E.; Dooley, D. M.; Mure, M.; Klinman, J. P. *Biochemistry* **1992**, *31*, 12147–12154. (c) Cooper, R. A.; Knowles, P. F.; Brown, D. E.; McGuirl, M. A.; Dooley, D. M. *Biochem. J.* **1992**, *288*, 337–340. (d) Brown, D. E.; McGuirl, M. A.; Dooley, D. M.; Janes, S. M.; Mu, D.; Klinman, J. P. *J. Biol. Chem.* **1991**, *266*, 4049–4051. (e) Mu, D.; Janes, S. M.; Smith, A. J.; Brown, D. E.; Dooley, D. M.; Klinman, J. P. *J. Biol. Chem.* **1992**, *267*, 7979–7982.
- (19) (a) Tommos, C.; Babcock, G. T. *Biochim. Biophys. Acta* **2000**, *1458*, 199–219. (b) Vrettos, J. S.; Limburg, J.; Brudvig, G. W. *Biochim. Biophys. Acta* **2001**, *1503*, 229–245. (c) Renger, G. *Biochim. Biophys. Acta* **2004**, *1655*, 195–204. (d) Rappaport, F.; Laverge, J. *Biochim. Biophys. Acta* **2001**, *1503*, 246–259. (e) Nugent, J. H. A.; Rich, A. M.; Evans, M. C. W. *Biochim. Biophys. Acta* **2001**, *1503*, 138–146. (f) Kuhne, H.; Brudvig, G. W. *J. Phys. Chem. B* **2002**, *106*, 8189–8196. (g) Faller, P.; Goussias, C.; Rutherford, A. W.; Un, S. *Proc. Natl. Acad. Sci. U.S.A.* **2003**, *100*, 8732–8735. (h) Ferreira, K. N.; Iverson, T. M.; Maghlaoui, K.; Barber, J.; Iwata, S. *Science* **2004**, *303*, 1831–1838. (i) Zouni, A.; Witt, H.-T.; Kern, J.; Fromme, P.; Krauss, N.; Saenger, W.; Orth, P. *Nature* **2001**, *409*, 739–743. (j) Rhee, K.-H.; Morris, E. P.; Barber, J.; Kuhlbrandt, W. *Nature* **1998**, *396*, 283–286. (k) Haumann, M.; Mulkidjanian, A.; Junge, W. *Biochemistry* **1999**, *38*, 1258–1267. (l) Kálmán, L.; LoBrutto, R.; Allen, J. P.; Williams, J. C. *Nature* **1999**, *402*, 696–699. (m) Petrouleas, V.; Koulouglotidis, D.; Ionnidis, N. *Biochemistry* **2005**, *44*, 6723–6728.
- (20) Graige, M. S.; Paddock, M. L.; Bruce, J. M.; Feher, G.; Okamura, M. Y. *J. Am. Chem. Soc.* **1996**, *118*, 9005–9016.
- (21) (a) Page, C. C.; Moser, C. C.; Chen, C.; Dutton, L. *Nature* **1999**, *402*, 47–5217. (b) Barbara, P. F.; Meyer, J. T.; Ratner, M. A. *J. Phys. Chem.* **1996**, *100*, 13148–13168.
- (22) Roth, J. P.; Yoder, J. C.; Won, T.-J.; Mayer, J. M. *Science* **2001**, *294*, 2524–2526.
- (23) (a) Swalina, C.; Pak, M. V.; Hammes-Schiffer, S. *Chem. Phys. Lett.* **2005**, *404*, 394–399. (b) Hammes-Schiffer, S.; Jordanova, N. *Biochim. Biophys. Acta* **2004**, *1655*, 29–36. (c) Hammes-Schiffer, S. *Acc. Chem. Res.* **2001**, *34*, 273–281. (d) Hammes-Schiffer, S. *ChemPhysChem* **2002**, *33*–42. (e) Cukier, R. I. *J. Phys. Chem. B* **2002**, *106*, 1746–1757. (f) Georgievskii, Y.; Stuchebrukhov, A. A. *J. Chem. Phys.* **2000**, *113*, 10438–10450. (g) Kuznetsov, A. M.; Ulstrup, J. *Can. J. Chem.* **1999**, *77*, 1085–1096. (h) Krishtalik, L. I. *Biochim. Biophys. Acta* **2000**, *1458*, 6–27. (i) References 1 and 2.
- (24) Rhile, I. J.; Mayer, J. M. *J. Am. Chem. Soc.* **2004**, *126*, 12718–12719.

Scheme 2. Synthesis of HOAr-NH₂

Scheme 2, following literature precedents.²⁵ The tertiary $-CPh_2NH_2$ and tBu substituents in the 2, 4, and 6 positions confer stability on the derived phenoxyl radical; 2,4,6- $tBu_3C_6H_2O^\bullet$, for instance, is stable in solution.²⁶ Recently, 2,4-di-*tert*-butyl-6-(*N*-methyl-2-pyrrolidyl)phenol was reported to give a persistent oxidized form, decaying over 30 min after bulk electrolysis.²⁷ Related compounds with a $-CH_2-$ spacer between the amine and the phenol are readily available via the Mannich reaction (phenol + formaldehyde + amine),²⁸ but such compounds are susceptible to radical attack at the benzylic hydrogens (and at other C–H bonds α to the amine).²⁹ The Mannich procedure cannot be used to make tertiary substituents because of the decreased reactivity of the ketone-derived iminium cation.²⁸ HOAr-NH₂ was therefore synthesized by addition of benzophenone to the lithiated phenol, leading to the *gem*-diphenyl substituents.^{25a} Subsequent trityl chemistry leads to products.^{25b,c} The corresponding chemistry with *gem*-methyl groups is diverted by elimination from the HOArCMe₂OH intermediate under the mild acidic conditions.

The related phenol with a 4,5-bis(4-anisyl)-2-imidazolyl substituent, HOAr-im, has been reported by Benisvy,³⁰ and the pyridyl compound HOAr-py has been prepared by Fujita.³¹ In each case, the authors explored the compounds' properties as ligands to metals. Both compounds fluoresce under ultraviolet light due to excited-state intramolecular proton transfer (ESIPT).³²

The X-ray crystal structures of HOAr-NH₂, HOAr-py, and HOAr-im (Figure 1) all show molecules with intramolecular hydrogen bonds from the phenol to the nitrogen base. There is some twisting between the phenol and pyridyl or imidazolyl rings, with inter-ring torsion angles of 22.6° for HOAr-im and

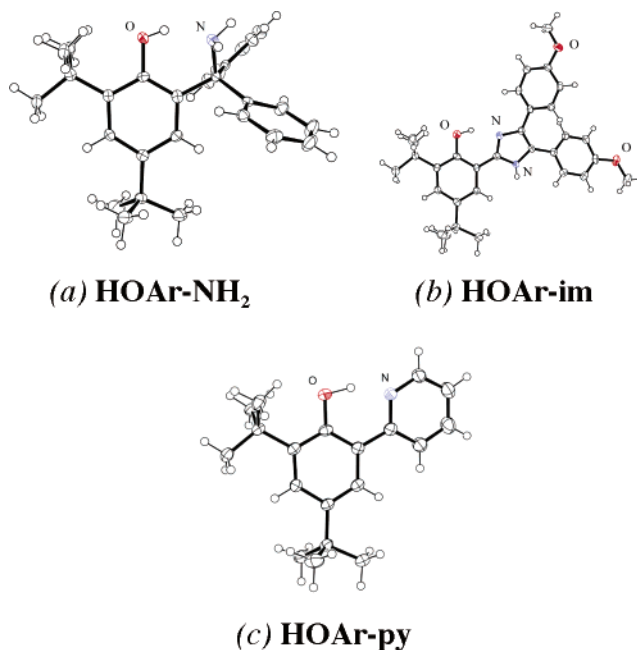


Figure 1. ORTEP drawings of (a) HOAr-NH₂, (b) HOAr-im, and (c) HOAr-py.

Table 1. Structural, Spectroscopic, and Electrochemical Data for Phenol–Base Compounds

phenol (HOAr-B)	$d_{O\cdots N}$ (Å)	δ_{O-H} (ppm) ^a	$E_{1/2}$ (V) [ΔE_p (mV)] ^b
HOAr-NH ₂	2.550(2), 2.613(3) ^c	12.32	0.37 [143] ^d
HOAr-im	2.646(2)	13.42	0.42 [105] ^e
HOAr-py	2.561(3), 2.567(3), 2.573(3) ^f	14.83	0.58 [100] ^d

^a ¹H NMR data in CD₃CN. ^b E vs Cp₂Fe⁺⁰. ^c Two independent molecules in the unit cell. ^d Scan rate = 200 mV s⁻¹. ^e Scan rate = 100 mV s⁻¹. ^f Three independent molecules in the unit cell.

11.9–15.4° for the three crystallographically independent molecules of HOAr-py. In the two independent molecules of HOAr-NH₂, the NCCC torsion angles are 33.4 and 42.0°. Similar structures have been observed for related molecules.³³ The O \cdots N distances across the hydrogen bond vary between 2.550(3) and 2.646(2) Å (Table 1), which are in the shorter portion of the known range for OH \cdots N hydrogen bonds.^{33,34} Crystal packing forces appear to play a significant role in these distances, as the two independent molecules of HOAr-NH₂ in the unit cell have O \cdots N distances that differ by 0.063 (4) Å; for the three molecules of HOAr-py, the O \cdots N distances vary by 0.012(3) Å. The imidazole derivative crystallizes with a molecule of methanol that is hydrogen-bonded to the imidazole NH hydrogen.

NMR spectra of the phenols in dry CD₃CN all show sharp downfield resonances for the phenolic proton, e.g., 12.32 ppm

- (25) (a) Talley J. J.; Evans, I. A. *J. Org. Chem.* **1984**, *49*, 5267–5269. (b) Gomberg, N.; Nishida, D. *J. Chem. Soc.* **1922**, 190–207. (c) Mandell, L.; Piper, J. V.; Pesterfield, C. E. *J. Org. Chem.* **1963**, *28*, 574–575.
- (26) Altwicker, E. R. *Chem. Rev.* **1967**, *67*, 475–531.
- (27) Maki, T.; Araki, Y.; Ishida, Y.; Onomura, O.; Matsumura, Y. *J. Am. Chem. Soc.* **2001**, *123*, 3371–3372.
- (28) (a) Tramontini, M.; Angiolini, L. *Tetrahedron* **1990**, *46*, 1791–1837. (b) Gevorgyan, G. A.; Agababyan, A. G.; Mndzhoyan, O. L. *Usp. Khim.* **1984**, *53*, 971–1013. (c) Tramontini, M. *Synthesis* **1973**, 703–775. (d) House, H. O. *Modern Synthetic Reactions*, 2nd ed.; W. A. Benjamin: New York, 1972; p 654. (e) See also refs 33a and 39.
- (29) Sparfel, D.; Baranne-Lafont, J.; Cuong, N. K.; Capdevielle, P.; Maumy, M. *Tetrahedron* **1990**, *46*, 803–814.
- (30) (a) Benisvy, L.; Bill, E.; Blake, A. J.; Collison, D.; Davies, E. S.; Garner, C. D.; Guindy, C. L.; McInnes, E. J. L.; McArdle, G.; McMaster, J.; Wilson, C.; Wolowska, J. *Dalton Trans.* **2004**, 3647–3653. (b) Benisvy, L.; Bittl, R.; Bothe, E.; Garner, C. D.; McMaster, J.; Ross, S.; Teutloff, C.; Neese, F. *Angew. Chem., Int. Ed.* **2005**, *44*, 5314–5317.
- (31) Inoue, Y.; Nakano, T.; Tanaka, H.; Kashiwa, N.; Fujita, T. *Chem. Lett.* **2001**, 1060–1061.
- (32) (a) Stolow, A. *Annu. Rev. Phys. Chem.* **2003**, *54*, 89–119. (b) LeGourrierec, D.; Kharlanov, V.; Brown, R. G.; Rettig, W. J. *Photochem. Photobiol. A* **1998**, *117*, 209–216. (c) Braeuer, M.; Mosquera, M.; Perez-Lustres, J. L.; Rodriguez-Prieto, F. *J. Phys. Chem. A* **1998**, *102*, 10736–10745.

- (33) (a) In Mannich bases, the range of O \cdots N distances across the hydrogen bond is 2.56–2.71 Å: Koll, A.; Wolschann, P. *Monatsh. Chem.* **1996**, *127*, 475–486. (b) Imidazoles, 2.55–2.60 Å: Foces-Foces, C.; Llames-Saiz, A. L.; Claramunt, R. M.; Cabildo, P.; Elguero, J. *J. Mol. Struct.* **1998**, *440*, 193–202. Benisvy, L.; Blake, A. J.; Collison, D.; Davies, E. S.; Garner, C. D.; McInnes, E. J. L.; McMaster, J.; Whittaker, G.; Wilson, C. *J. Chem. Soc., Dalton Trans.* **2003**, 1975–1985. (c) Pyridines, 2.54–2.56 Å: Shu, Wenmao; Valiyaveetil, S. *Chem. Commun.* **2002**, 1350–1351. Kaczmarek, L.; Balicki, R.; Lipowski, J.; Borowicz, P.; Grabowska, A. *J. Chem. Soc., Perkin Trans. 2* **1994**, 1603–1610. (d) Most Mannich bases HOAr-CH₂-NR₂ are nonplanar due to steric pressure from the R groups.^{33a-c,75}
- (34) (a) Pimental, G. C.; McClellan, A. L. *The Hydrogen Bond*; Freeman: New York, 1960. (b) Frey, P. A. *Magn. Reson. Chem.* **2001**, *39*, S190–S198. (c) Gilli, P.; Bertolasi, V.; Gilli, G. *J. Am. Chem. Soc.* **2000**, *122*, 10405–10417.

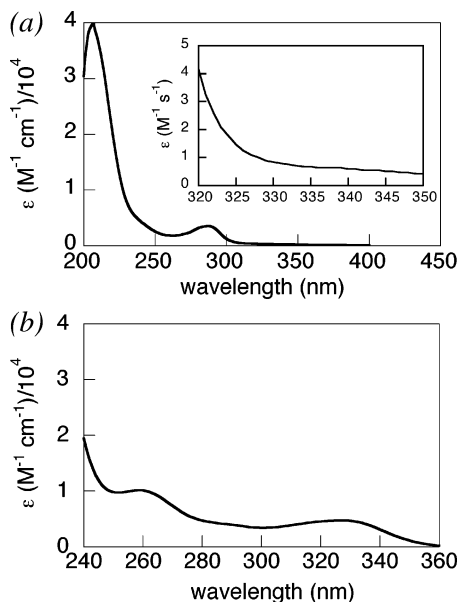
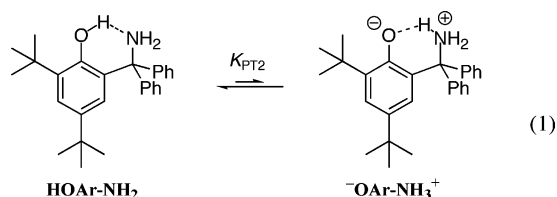


Figure 2. UV-vis spectra of (a) phenol **HOAr-NH₂** and (b) phenoxide **-OAr-NH₂** in MeCN. The inset of spectrum (a) is the spectrum of a saturated solution of **HOAr-NH₂** in a 10 cm path length cell.

for **HOAr-NH₂**, typical of intramolecularly hydrogen-bonded phenols.^{35a} The chemical shifts for **HOAr-py** (14.83 ppm) and **HOAr-im** (13.42 ppm) are farther downfield, as has been previously observed for related compounds³⁶ that have “resonance-assisted hydrogen bonds” due to the conjugation between the phenol and the basic site.^{34c,37} The two *p*-anisyl groups in **HOAr-im** are inequivalent, indicating that intermolecular proton transfer between imidazole nitrogen atoms is slow on the NMR time scale, presumably due in part to the strong OH...N hydrogen bond.

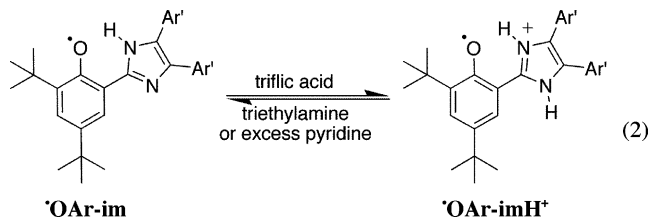
The UV-vis spectrum of **HOAr-NH₂** contains absorptions typical of aromatic compounds^{35b} at 207 (40 000) and 287 nm (3600) (Figure 2a; the ϵ value is stated parenthetically after each λ_{\max} in $\text{M}^{-1} \text{cm}^{-1}$). The deprotonated phenol (**-OAr-NH₂**) is generated in MeCN by addition of excess di(*n*-butylammonium) succinate.³⁸ **-OAr-NH₂** has additional absorptions at 259 (6900) and 327 nm (4700) (Figure 2b), low-energy absorptions that are typical of phenoxides.³⁵ A UV-vis spectrum of a saturated (16.0 mM) MeCN solution of **HOAr-NH₂** in a 10.00 cm quartz cell shows no absorption maximum in the phenoxide region (inset of Figure 2a). These optical spectra provide an estimate of the equilibrium constant K_{PT2} for formation of the zwitterion **-OAr-NH₃⁺** (eq 1). Mannich bases with strongly acidic phenols can exist in this tautomeric form, and the optical spectrum of the phenoxide (e.g., **-OAr-NH₂**) has often been taken as a model for the low-energy part of the spectrum of the zwitterion.³⁹ With this assumption, the lack of an absorption maximum at 327 nm ($\epsilon_{\text{HOAr-NH}_2(327)} = 1.1 \text{ M}^{-1} \text{cm}^{-1}$) implies that essentially no zwitterion is present in MeCN solution, that $K_{\text{PT2}} < 10^{-4}$. Similarly, the UV-vis spectrum of



HOAr-py shows no peak above 385 nm that would be characteristic of the proton-transferred structure.⁴⁰

2. Cyclic Voltammetry and Chemical Oxidations. Oxidations of **HOAr-NH₂**, **HOAr-im**, and **HOAr-py** with near-stoichiometric amounts of $[\text{N}(p\text{-C}_6\text{H}_4\text{Br})_3]^+$ yield the corresponding phenoxyl radical (Scheme 1 above), as confirmed by both UV-vis and ¹H NMR spectroscopies (at $\sim 10 \mu\text{M}$ and $\sim 1 \text{ mM}$ concentrations, respectively). The reactions are marked by a rapid decrease of the intense absorption of the blue aminium ion at 699 nm ($40\,000 \text{ M}^{-1} \text{cm}^{-1}$). These reactions, and most of the solution measurements in this report, were done in MeCN.

Oxidation of **HOAr-im** with $[\text{N}(p\text{-C}_6\text{H}_4\text{Br})_3]^+$ yields a blue solution of **•OAr-imH⁺** with an absorption at 695 nm (8300) which decays to $\sim 33\%$ intensity over 1.5 h. Phenoxyl radicals typically have absorptions between 420 and 720 nm, with higher intensity for the more conjugated radicals [λ_{\max} , nm (ϵ , $\text{M}^{-1} \text{cm}^{-1}$): 2,4,6-tri-*tert*-butylphenoxy radical (**•Bu₃ArO•**), 630 (400), benzene;⁴¹ 2,6-*t*-Bu₂-4-Ph-C₆H₂OH, 488 (2780); 2,6-*t*-Bu₂-4-(Me₂NC₆H₄)C₆H₂OH, 650 (6000)].²⁶ Treating **•OAr-imH⁺** in MeCN with triethylamine or excess pyridine ($\text{p}K_{\text{a}} = 18, 12$, respectively³⁸) produces a purple solution with $\lambda_{\max} = 544 \text{ nm}$ (approximately 6100) due to the deprotonated phenoxyl radical **•OAr-im** (Figure 3, eq 2). This species likely still has an



intramolecular hydrogen bond from the imidazole hydrogen to the oxyl radical. **•OAr-im** was prepared independently by heterogeneous PbO_2 oxidation of **HOAr-im** in MeCN or DMSO.⁴² This isolated **•OAr-im** had an absorption at 544 nm and contained some **HOAr-im** by ¹H NMR. Addition of 1 equiv of triflic acid to solutions of **•OAr-im** formed the 695 nm absorption characteristic of **•OAr-imH⁺** (eq 2).

Oxidation of **HOAr-py** by $[\text{N}(p\text{-C}_6\text{H}_4\text{Br})_3]^+$ gives a yellow solution with $\lambda_{\max} = 481 \text{ nm}$ (1600), which fades with $t_{1/2} \approx 6$

- (35) Silverstein, R. M.; Bassler, G. C.; Morrill, T. C. *Spectrometric Identification of Organic Compounds*, 5th ed.; Wiley: New York, 1991; (a) p 184 and (b) pp 306–311.
 (36) Rozwadowski, Z.; Majeewski, E.; Dziembowska, T.; Hansen, P. *J. Chem. Soc., Perkin Trans. 2* **1999**, 2809–2817.
 (37) Gilli, G.; Belluci, F.; Ferretti, V.; Bertolasi, V. *J. Am. Chem. Soc.* **1989**, *111*, 1023–1028.
 (38) Izutsu, K. *Acid-Base Dissociation Constants in Dipolar Aprotic Solvents*; IUPAC Chemical Data Series No. 35; Blackwell Scientific Publications: Boston, MA, 1990; pp 17–35. The $\text{p}K_{\text{a2}}$ of succinic acid in MeCN is 29.0.

- (39) (a) Koll, A.; Wolschann, P. *Monatsh. Chem.* **1999**, *130*, 983–1001. (b) Przeslawska, M.; Koll, A.; Witanowski, M. *J. Phys. Org. Chem.* **1999**, *12*, 486–492. (c) Teitelbaum, A. B.; Derstuganova, K. A.; Shishkina, N. A.; Kudryavtseva, L. A.; Bel'skii, V. E.; Ivanov, B. E. *Bull. Acad. Sci. USSR, Div. Chem. Sci. (Engl. Transl.)* **1980**, 558–562; *Izv. Akad. Nauk SSSR, Ser. Khim.* **1980**, 803–808.
 (40) (a) Król-Starzomska, I.; Filarowski, A.; Rospenk, M.; Koll, A. *J. Phys. Chem. A* **2004**, *108*, 2131–2138. This work states that zwitterionic *o*-hydroxy Schiff bases have $385 \text{ nm} < \lambda_{\max} < 430 \text{ nm}$. (b) Popp, G. *J. Org. Chem.* **1972**, *37*, 3058–3062. (c) Lapachev, V.; Stekhova, S.; Mamaev, V. *Monatsh. Chem.* **1987**, *118*, 669–670.
 (41) (a) Woon, T. C.; Dicken, C. M.; Bruce, T. C. *J. Am. Chem. Soc.* **1986**, *108*, 7990–7995. (b) Pokhodenko, V. D.; Khizhny, V. A.; Koshechko, V. G.; Samarskii, V. A. *Theor. Exp. Chem. (Engl. Transl.)* **1975**, *11*, 489–493; *Teor. Eksper. Khim.* **1975**, *11*, 579–584. This work reports **•Bu₃ArO•** λ_{\max} (nm, MeCN) = 316, 628 nm (but no ϵ 's).
 (42) (a) Xie, C.; Lahti, P. M. *Tetrahedron Lett.* **1999**, *40*, 4305–4308. (b) Xie, C.; Lahti, P. M.; George, C. *Org. Lett.* **2000**, *2*, 3417–3420.

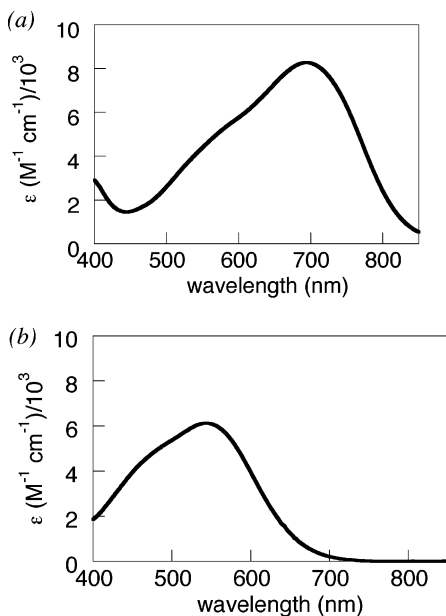


Figure 3. Visible spectra of (a) $\bullet\text{OAr-imH}^+$ and (b) $\bullet\text{OAr-im}$ in MeCN.

h. Reactions of HOAr-NH_2 with $[\text{N}(p\text{-C}_6\text{H}_4\text{Br})_3]^{*+}$ show no absorptions above 400 nm at 100 μM , indicating a colorless radical product. A complex EPR spectrum was recorded for one of the oxidation mixtures of HOAr-NH_2 in CH_2Cl_2 (see Supporting Information of ref 24). ^1H NMR monitoring of reactions of HOAr-NH_2 with substoichiometric amounts of $[\text{N}(p\text{-C}_6\text{H}_4\text{Br})_3]^{*+}$ in MeCN showed reduced signals for HOAr-NH_2 and the appearance of $\text{N}(p\text{-C}_6\text{H}_4\text{Br})_3$. With excess $[\text{N}(p\text{-C}_6\text{H}_4\text{Br})_3]^{*+}$, the amine is not observed because there is rapid exchange between NAr_3 and $[\text{NAr}_3]^{*+}$ by electron transfer.⁴³

The cyclic voltammograms of the three phenols in 0.1 M $n\text{Bu}_4\text{NPF}_6/\text{MeCN}$ (Table 1, Figures 4a and S20 in Supporting Information) are quasi-reversible, with almost equal anodic and cathodic currents but with peak separations (ΔE_p) larger than the theoretical 59 mV. The rate constant for heterogeneous electron transfer (k_{el}) for HOAr-NH_2 has been determined by analysis of the CV data at different scan rates ν (Figure 4a).⁴⁴ k_{el} is related to ΔE_p and ν by eqs 3 and 4,

$$k_{\text{el}}^0 = \psi \left(\frac{\pi D_{\text{O}} F \nu}{RT} \right)^{1/2} \left(\frac{D_{\text{R}}}{D_{\text{O}}} \right)^{\alpha/2} \quad (3)$$

$$\ln \psi = 3.69 - 1.16 \ln(\Delta E_p - 59) \quad (4)$$

where D_{O} and D_{R} are the diffusion constants ($\text{cm}^2 \text{s}^{-1}$) for the oxidized and reduced forms of the analyte, α is the transfer coefficient (taken to be 0.5⁴⁵), and R and T have their standard meanings. A , D_{O} , and D_{R} were determined using chronoamperometry (see Supporting Information). k_{el} was found to be $(3 \pm 1) \times 10^{-3} \text{ cm s}^{-1}$ from the slope of a plot of ψ vs $\nu^{-1/2}$ (Figure 4b). To support our measurements, these parameters were used to simulate the CVs using DigiSim⁴⁶ with good results (inset, Figure 4a). For comparison, Evans, Savéant, and co-workers

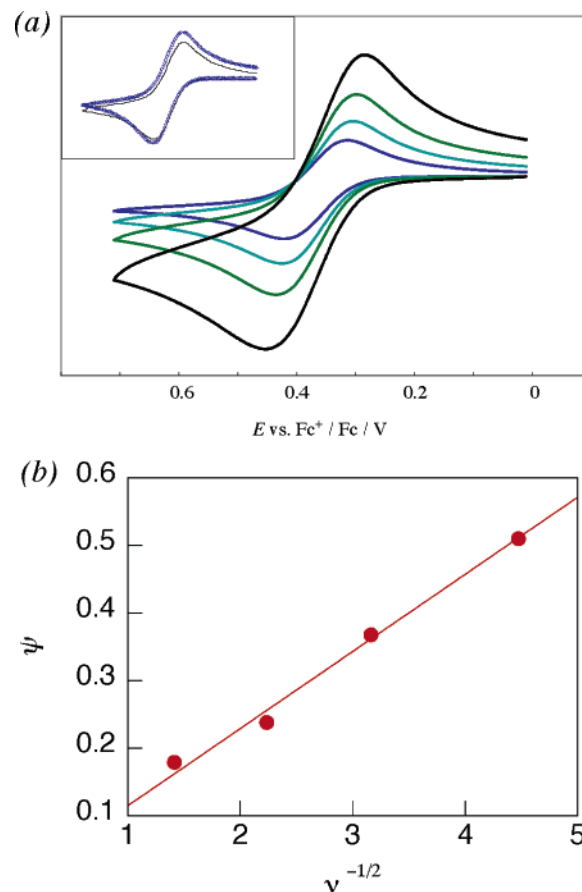


Figure 4. (a) Cyclic voltammograms of HOAr-NH_2 with $\nu = 0.05, 0.1, 0.2,$ and 0.5 V s^{-1} . Inset: An overlay of the simulated (blue dots) and experimental CVs at 100 mV s^{-1} . (b) Plot of ψ vs $\nu^{-1/2}$ for HOAr-NH_2 (see eqs 3 and 4 in text).

have recently reported a much slower heterogeneous rate constant of $(9 \pm 5) \times 10^{-7} \text{ cm s}^{-1}$ for CPET reduction of a water–superoxide complex, which exhibits a much more distorted cyclic voltammogram.⁴

Similar quasi-reversible voltammograms have been reported for other phenols with intra- or intermolecularly hydrogen-bonded amine or pyridine bases.^{7,27,30,47} In contrast, electrochemical oxidations of phenols without an attached base are irreversible in dried aprotic solvents, occurring via an EC mechanism. The chemical step (“C”) is typically proton transfer into the bulk solution, which is effectively irreversible in aprotic media.⁴⁸ Thus, oxidation of 2,4,6- $t\text{Bu}_3\text{ArOH}$ is irreversible in dry MeCN, even though the radical 2,4,6- $t\text{Bu}_3\text{ArO}\bullet$ is stable.^{48a} Matsumura et al. have shown²⁷ that moving the attached base from the ortho to the para position changes the oxidation from quasi-reversible to irreversible. Oxidation of the methyl ether MeOAr-NH_2 is irreversible ($E_{\text{p,a}} = 1.2 \text{ V}$; all potentials in this report are vs $\text{Cp}_2\text{Fe}^{0/+}$ in MeCN), probably because without the stabilizing proton transfer the high-energy anisyl or aminium radical cation decays rapidly. The related phenol–alcohol

(43) Sorensen, S. P.; Bruning, W. H. *J. Am. Chem. Soc.* **1973**, *95*, 2445–2451.

(44) (a) Swaddle, T. W. *Chem. Rev.* **2005**, *105*, 2573–2608. (b) Bard, A. J.; Faulkner, L. R. *Electrochemical Methods: Fundamentals and Applications*, 2nd ed.; John Wiley and Sons Inc.: New York, 2001.

(45) The value of ψ is nearly independent of α ($0.3 < \alpha < 0.7$) (Nicholson, R. S. *Anal. Chem.* **1965**, *37*, 1351). When $i_{\text{pc}}/i_{\text{pa}} = 1$, as is the case here, the value of α is typically close to 0.5. Simulated CVs using $\alpha = 0.4, 0.5,$ and 0.6 showed no significant difference.

(46) DigiSim software is a product of Bioanalytical Systems, Inc. (<http://www.bioanalytical.com/products/ec/digisim/index.html>).

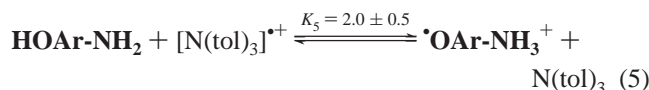
(47) (a) Thomas, F.; Jarjays, O.; Jamet, H.; Hamman, S.; Saint-Aman, E.; Duboc, C.; Pierre, J.-L. *Angew. Chem.* **2004**, *116*, 604–607; *Angew. Chem., Int. Ed.* **2004**, *43*, 594–597. (b) Rhile, I. J.; Mayer, J. M. *Angew. Chem.* **2005**, *105*, 1624–1625; *Angew. Chem., Int. Ed.* **2005**, *44*, 1598–1599.

(48) (a) Bordwell, F. G.; Cheng, J.-P. *J. Am. Chem. Soc.* **1991**, *113*, 1736–1743. (b) Cf.: Williams, L. L.; Webster, R. D. *J. Am. Chem. Soc.* **2004**, *126*, 12441–12450. (c) For aqueous electrochemistry, see: Li, C.; Hoffman, M. Z. *J. Phys. Chem. B* **1999**, *103*, 6653–6656.

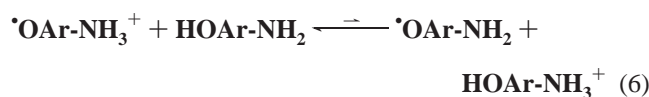
HOAr-OH [(2-CPh₂OH)(4,6-^tBu₂)C₆H₂OH] also shows irreversible electrochemistry ($E_{p,a} = 1.1$ V), possibly because proton transfer to the weakly basic primary alcohol is not favored and the proton is lost to the bulk solution. CV of the phenoxide **HOAr-NH₂**, as the ^tBu₄N⁺ salt, shows a reversible oxidation wave centered at -0.57 V, essentially equal to the $E_{1/2}$ for 2,4,6-tri-^t-butylphenoxide, -0.572 V.^{48a,53}

The average of the anodic and cathodic peaks for **HOAr-NH₂**, **HOAr-im**, and **HOAr-py** is taken as the $E_{1/2}$ for the coupled proton–electron transfer (CPET), the potential for transfer of both an electron to the electrode and the phenolic proton to the amine (Scheme 1). This is the interpretation of most of the previous electrochemical studies of phenol–base systems.^{7,27,30} One recent paper has interpreted the large ΔE_p for oxidation of a phenol–amine as indicating a stepwise EC (ET–PT) mechanism,^{47a} but this is, in our view, inappropriate.^{47b} The assignment of $E_{1/2}$ as the energetics of CPET is supported by the thermodynamic discussion below and by the following equilibration experiment.

Oxidation of **HOAr-NH₂** by [N(tol)₃]⁺ yields an equilibrium mixture with the phenoxyl radical and the tri-*p*-tolylamine, with equilibrium constant K_5 (eq 5). Addition of N(tol)₃ to the



reaction mixture causes an increase in the optical absorbance due to [N(tol)₃]⁺, yielding $K_5 = 2.4$. Alternatively, addition of aliquots of triflic acid to solutions containing large excesses of N(tol)₃ and **HOAr-NH₂** versus [N(tol)₃]⁺ quantitatively protonates **HOAr-NH₂** and therefore shifts the equilibrium toward [N(tol)₃]⁺. This experiment afforded $K_5 = 1.5$, and also established that a second proton transfer equilibrium, eq 6, is not significant ($K_6 \ll 1$).⁴⁹ It should be noted that these



equilibrium experiments are possible only because of the stability of the phenoxyl radical on the chemical time scale. Together, the equilibria establish an overall equilibrium constant $K_5 = 2.0 \pm 0.5$, which implies a difference in redox potential between $E(\text{HOAr-NH}_2^{+/0})$ and $E([\text{N}(\text{tol})_3]^{+/0})$ of 18 ± 8 mV. This is in excellent agreement with the 20 ± 30 mV difference in the electrochemical $E_{1/2}$ values: 0.36 ± 0.02 V for **HOAr-NH₂**^{+/0} and 0.38 ± 0.02 V for [N(tol)₃]^{+/0}. The agreement validates the assignment of the phenol $E_{1/2}$ values as $E(\text{CPET})$.

The oxidants used in this study include variously substituted triarylammonium ions [N(*p*-C₆H₄X)₃]⁺, iron(III) tris-polyridyl complexes [Fe(N–N)₃]³⁺ (N–N = 2,2′-bipyridine or 1,10-

Table 2. Potentials of Oxidants (in MeCN, V vs Cp₂Fe^{+/0})^a

oxidant	$E_{1/2}$
[N(<i>p</i> -C ₆ H ₄ Br) ₃] ⁺	0.67
[N(<i>p</i> -C ₆ H ₄ OMe)(<i>p</i> -C ₆ H ₄ Br) ₂] ⁺	0.48
[N(tol) ₃] ⁺ ^b	0.38
[N(<i>p</i> -C ₆ H ₄ OMe) ₂ (<i>p</i> -C ₆ H ₄ Br)] ⁺	0.32
[N(<i>p</i> -C ₆ H ₄ OMe) ₃] ⁺	0.16
[Fe(bpy) ₃] ³⁺	0.70
[Fe(5,5′-Me ₂ bpy) ₃] ³⁺	0.58
[Fe(4,7-Me ₂ phen) ₃] ³⁺	0.53
[Fe(3,4,7,8-Me ₄ phen) ₃] ³⁺	0.46
[MPT] ^{+/+} ^c	0.32

^a See Experimental Section for conditions. ^b Tri-*p*-tolylammonium. ^c 10-Methylphenothiazinium.

phenanthroline derivative), and the 10-methylphenothiazinium ion [MPT]^{+/+}. All displayed reversible cyclic voltammograms (Table 2). The [Fe(N–N)₃]^{3+/2+} potentials in MeCN vary substantially with ionic strength due to differences in ion-pairing between the Fe^{II} and Fe^{III} forms.⁵⁰ For [Fe(5,5′-Me₂bpy)₃]^{3+/2+}, the potential changes by -40 ± 4 mV/log(*i*). Kinetic studies using [Fe(R₂bpy)₃]³⁺ and [Fe(Me₂phen)₃]³⁺ were done at 0.1 M ionic strength to match the electrochemical conditions. For the singly charged [N(tol)₃]^{+/+}, the change in potential with ionic strength was found to be minimal [3 ± 1 mV/log(*i*)].

3. Kinetics. The rates of oxidation of the phenols have been monitored by stopped-flow kinetics, following the disappearance of the oxidant in reactions of [NAr₃]^{+/+} or the appearance of [Fe(N–N)₃]²⁺ in reactions with iron oxidants. Reactions of the iron complexes were performed in MeCN containing 0.1 M ^tBu₄NPF₆ to match the electrochemical conditions (see above). When possible, reactions were performed with a large excess of phenol relative to oxidant (>5 equiv).

The time sequences of optical spectra were globally analyzed to derive rate constants using SPECFIT software⁵¹ (or, in one instance,⁴⁹ Microsoft Excel) (Table 3). For thermodynamically favorable reactions ($K_{\text{eq}} \gg 1$) run under pseudo-first-order conditions, the second-order rate constant was taken as the slope of a plot of k_{obs} vs [HOAr-B]. Particularly fast reactions were analyzed with second-order kinetics, and reactions with $K_{\text{eq}} \lesssim 1$ were analyzed as opposing second-order reactions. In each case, the rate constant was derived from approximately 25 kinetic runs, at five different concentrations. The temperature dependence of the rate constants was measured over 30–47 K ranges (Figure 5), yielding the Eyring parameters⁵² in Table 4 (below). Variations in driving force over the appropriate temperature ranges for the reactions of **HOAr-NH₂** + [N(tol)₃]^{+/+} and **HOAr-py** + [Fe(5,5′-Me₂bpy)₃]³⁺ were evaluated by cyclic voltammetry of the individual reagents. The difference between the half-reaction potentials measured at 2 and 46 °C (for **HOAr-py** and [Fe(5,5′-Me₂bpy)₃]³⁺) or 49 °C (for **HOAr-NH₂** and [N(tol)₃]^{+/+}) were found to be within the propagated experimental error (± 30 mV).

To determine the kinetic isotope effects, MeCN solutions of **HOAr-NH₂** and **HOAr-py** were prepared with 0.5–1% v/v CH₃OD and the kinetics performed otherwise as above. The large molar excess of CH₃OD provided high isotopic enrichment at the exchangeable OH and NH₂ positions (the rate constants were corrected for the residual proton content in the CH₃OD). Control experiments showed that addition of 1% v/v protio-methanol (CH₃OH) does not affect the rate constant for these reactions. $k_{\text{HOAr-NH}_2}/k_{\text{DOAr-ND}_2}$ ranges from 1.6 ± 0.2 to $2.6 \pm$

(49) See the Supporting Information of ref 24.

(50) (a) Noel, M.; Vasu, K. I. *Cyclic Voltammetry and the Frontiers of Electrochemistry*; Aspect: London, 1990; pp 141–143. (b) Braga, T. G.; Wahl, A. C. *J. Phys. Chem.* **1985**, *89*, 5822–5828. (c) Chan, M.-S.; Wahl, A. C. *J. Phys. Chem.* **1978**, *82*, 2542–2549.

(51) Binstead, R. A.; Zuberbühler, A. D.; Jung, B. *Specfit*, version 3.0.36 (32-bit Windows); Spectrum Software Associates: Chapel Hill, NC, 2004.

(52) Eyring equation: $k = \kappa(k_B T/h) \exp[(T\Delta S^\ddagger - \Delta H^\ddagger)/RT]$; κ is assumed to be 1.

(53) (a) From ref 48a, $E(2,4,6\text{-}^t\text{Bu}_3\text{ArOH}) = 1.85$ V in MeCN vs Ag/AgI in MeCN and $E_{\text{Ag}/\text{Ag}^+} = E_{\text{SCE}} + 0.365$ V. Using $E_{\text{Fe}/\text{Fe}^{3+}} = E_{\text{SCE}} - 0.40$ V (ref 53b), the potential for **Bu₃ArOH** in MeCN is 1.09 V vs Cp₂Fe^{+/0}. (b) Connelly, N. G.; Geiger, W. E. *Chem. Rev.* **1996**, *96*, 877–910.

Table 3. Rate Constants for Phenol Oxidations (295 ± 2 K, MeCN)

phenol	oxidant ^a	k (M ⁻¹ s ⁻¹)	E_{ox}^b (V)
HOAr-NH₂	[Fe(bpy) ₃] ³⁺	(4 ± 1) × 10 ⁶	0.34
	[N(<i>p</i> -C ₆ H ₄ Br) ₃] ³⁺	(4 ± 2) × 10 ⁷	0.31
	[Fe(5,5′-Me ₂ bpy) ₃] ³⁺	(1.5 ± 0.2) × 10 ⁵	0.22
	[Fe(4,7-Me ₂ phen) ₃] ³⁺	(3.8 ± 0.4) × 10 ⁵	0.16
	[N(<i>p</i> -C ₆ H ₄ OMe)(<i>p</i> -C ₆ H ₄ Br) ₂] ³⁺	(8 ± 1) × 10 ⁵	0.12
	[Fe(3,4,7,8-Me ₄ phen) ₃] ³⁺	(3.0 ± 0.3) × 10 ⁴	0.09
	[N(tol) ₃] ³⁺	(1.1 ± 0.2) × 10 ⁵	0.02
	[N(<i>p</i> -C ₆ H ₄ OMe) ₃] ³⁺	(1.1 ± 0.1) × 10 ³	-0.20
	[N(<i>p</i> -C ₆ H ₄ OMe) ₂ (<i>p</i> -C ₆ H ₄ Br)] ³⁺	(2.7 ± 0.3) × 10 ⁴	-0.04
	[MPT] ³⁺	(3.2 ± 0.3) × 10 ⁴	-0.04
DOAr-ND₂^c	[Fe(5,5′-Me ₂ bpy) ₃] ³⁺	(5.8 ± 0.6) × 10 ⁴	0.22
		$k_{\text{H}}/k_{\text{D}} = 2.6 \pm 0.4^d$	
	[N(tol) ₃] ³⁺	(4.3 ± 0.4) × 10 ⁴	0.02
		$k_{\text{H}}/k_{\text{D}} = 2.5 \pm 0.3^d$	
	[N(<i>p</i> -C ₆ H ₄ OMe) ₃] ³⁺	(6.9 ± 0.7) × 10 ²	-0.20
		$k_{\text{H}}/k_{\text{D}} = 1.6 \pm 0.2^d$	
HOAr-im	[N(<i>p</i> -C ₆ H ₄ OMe) ₃] ³⁺	(1.1 ± 0.1) × 10 ⁴	-0.26
	HOAr-py	[Fe(bpy) ₃] ³⁺	(5.2 ± 0.8) × 10 ⁶
	[Fe(5,5′-Me ₂ bpy) ₃] ³⁺	(5.8 ± 0.9) × 10 ⁵	0.00
	[Fe(4,7-Me ₂ phen) ₃] ³⁺	(1.9 ± 0.4) × 10 ⁶	-0.05
	[Fe(3,4,7,8-Me ₄ phen) ₃] ³⁺	(3.3 ± 0.6) × 10 ⁵	-0.12
DOAr-py^c	[Fe(bpy) ₃] ³⁺	(1.5 ± 0.2) × 10 ⁶	0.12
		$k_{\text{H}}/k_{\text{D}} = 2.8 \pm 0.6$	
	[Fe(5,5′-Me ₂ bpy) ₃] ³⁺	(2.3 ± 0.4) × 10 ⁵	0.00
		$k_{\text{H}}/k_{\text{D}} = 2.5 \pm 0.6$	

^a Reactions with [Fe(N–N)₃]³⁺ were performed in 0.1 M Bu₄NPF₆/MeCN. ^b $E_{\text{rxn}} = E_{1/2}(\text{oxidant}) - E_{1/2}(\text{phenol})$. ^c Reactions with deuterated substrates were performed in 0.5–1% v/v CH₃OD in MeCN. Rate constants are corrected for residual proton content using $k_{\text{expt}} = k_{\text{D}}(1 - f_{\text{H}}) + f_{\text{H}}k_{\text{H}}$, where f_{H} is the fraction protonated. ^d $k_{\text{HOAr-NH}_2}/k_{\text{DOAr-ND}_2}$.

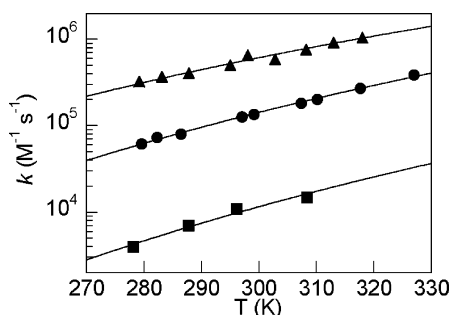


Figure 5. Temperature dependence of the rate constants for **HOAr-py** + [Fe(5,5′-Me₂bpy)₃]³⁺ (▲), **HOAr-NH₂** + [N(tol)₃]³⁺ (●), and **HOAr-im** + [N(C₆H₄OMe)₃]³⁺ (■). The curve fits are to the non-adiabatic form of the Marcus equation (eq 15; see Discussion).

0.4 and $k_{\text{HOAr-py}}/k_{\text{DOAr-py}} = 2.5 \pm 0.6$ or 2.8 ± 0.6 , depending on the oxidant (Table 3).

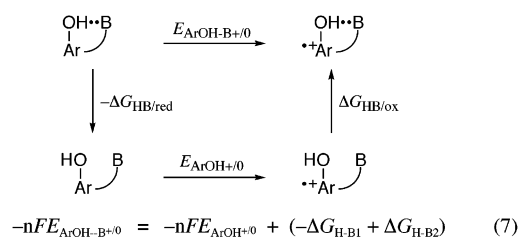
Discussion

Phenols with an intramolecular hydrogen bond react with one-electron oxidants to generate phenoxyl radicals in which the proton has transferred. The phenols and phenoxyl radicals have been characterized by spectroscopy, cyclic voltammetry, and chemical reactivity. The kinetics of oxidation have been examined for a number of phenol–oxidant pairs, in one case electrochemically. We discuss first the thermochemistry of outersphere oxidation of these phenols, and then the mechanistic data that implicate a concerted proton–electron transfer (CPET) pathway for the reactions. Finally, analysis of the CPET rate constants indicates that the classical Marcus theory is an excellent starting point to understand these processes.

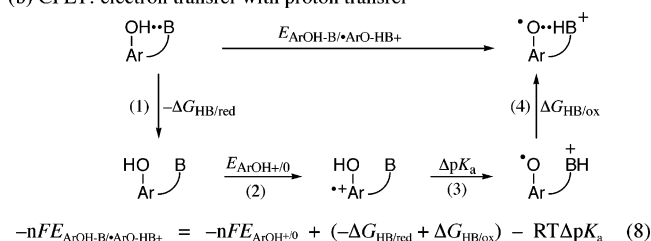
1. Phenol Potentials. The potentials for **HOAr-B** (0.36–0.58 V vs Cp₂Fe⁺⁰ in MeCN, Table 1) are significantly lower than reported values for one-electron oxidation of phenols without a pendant base. 2,4,6-Tri-*tert*-butylphenol, for example,

Scheme 3. Thermochemical Cycle Indicating the Effect of Hydrogen Bonding on Redox Potentials

(a) Electron transfer without proton transfer



(b) CPET: electron transfer with proton transfer



has $E_{\text{p,a}}(\text{Bu}_3\text{ArOH}^{+0}) = 1.09$ V.⁵³ Such large shifts have been suggested to be due to hydrogen-bonding effects, but the analysis below shows that the shifts must be due to proton transfer.⁴⁷

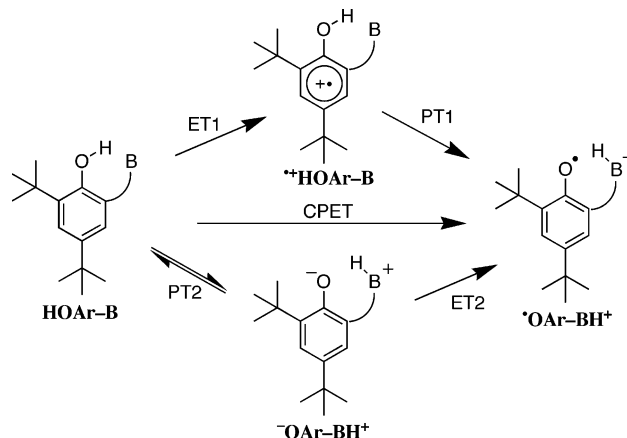
Consider the oxidation of a phenol hydrogen-bonded to a base B by electron transfer without proton transfer. The effect of the hydrogen bonding is illustrated by the thermochemical cycle in Scheme 3a, which compares the potentials for the H-bonded and non-H-bonded forms ($E_{\text{ArOH-B}+0}$, $E_{\text{ArOH}+0}$). The difference between these two potentials is equal to the difference in the strengths of the hydrogen bonds in the reduced and oxidized forms ($\Delta G_{\text{HB/red}} - \Delta G_{\text{HB/ox}}$) (eq 7). Note that the absolute hydrogen bond strengths are not important, only the change upon oxidation. Since most hydrogen bonds are 3–8 kcal mol⁻¹,⁵⁴ shifts of more than ca. 5 kcal mol⁻¹ (0.2 V) would be quite

unusual. A very recent experimental study in general supports these thermochemical arguments.⁵⁵

The effect of the hydrogen bonding on a CPET redox potential is similar. Progressing around the thermochemical cycle in Scheme 3b, (1) the hydrogen bond in **HOAr-B** is broken ($-\Delta G_{\text{HB/red}}$); (2) the non-hydrogen-bonded phenol is oxidized ($E_{\text{ArOH}^{+0}}$); (3) the proton is transferred ($-RT\Delta pK_a$); and (4) the hydrogen bond of **•OAr-BH⁺** is formed ($\Delta G_{\text{HB/ox}}$). The sum of these four steps is equal to the overall potential (eq 8). For the sterically crowded phenols discussed here, $E_{\text{ArOH}^{+0}}$ is probably well approximated by the **•Bu₃ArOH⁺⁰** potential.⁵⁶ With this approximation, the difference between the potential for **•OAr-BH⁺**/**HOAr-B** and that for **•Bu₃ArOH⁺⁰** is the energetics of the proton-transfer step ($-RT\Delta pK_a$) plus the difference in hydrogen bond strengths. As in the pure electron transfer case of Scheme 3a, it is the change in H-bond strengths rather than their absolute value that is important.

The change in hydrogen bond strength and the attendant shift of the redox potential is likely to be quite small. As noted above, the hydrogen-bonded phenoxide **•OAr-NH₂** has the same potential as the non-H-bonded 2,4,6-**•Bu₃ArO⁻**. The potentials for **•Bu₃ArOH** (+1.09 V), the anisole **MeOAr-NH₂** (~1.2 V), and the hydroxyphenol **HOAr-OH** (~1.1 V) are quite similar, despite what are likely very different H-bonds (OH...NCMe, O...HN, and OH...OH). Hammarström and co-workers attribute 0.10 V (2 kcal mol⁻¹) to the change in hydrogen bonding for the tyrosine-histidine pair in their model system.⁵⁷ Phenoxyl radicals are known to make strong hydrogen bonds in some systems,⁵⁸ so the H-bond in **•OAr-BH⁺** could be stronger than that in **HOAr-B**, but this effect is usually small. The H-bond strengthening upon oxidation of catechols to oxyl radicals has been variously estimated as between ~4 and <1 kcal mol⁻¹.⁵⁸ The strengthening in catechols and 1,8-naphthalenediols is particularly large because oxidation yields hydrogen bonds in which PT is degenerate; one report describes a ~7 kcal mol⁻¹ (0.3 eV) strengthening for 1,8-naphthalenediols.^{58d} For the case of **HOAr-NH₂**, the hydrogen bond could be even stronger in the neutral phenol because of the much larger pK_a mismatch between donor and acceptor in the radical cation.⁵⁹ This would shift the potential in the opposite direction.

Scheme 4. Three Possible Mechanisms for Oxidation of Phenol-Base Compounds



In sum, the difference of 0.5–0.7 V in redox potentials for **HOAr-B** vs **•Bu₃ArOH⁺⁰** is too large to be due to changes in hydrogen bond strength. This difference is primarily due to the proton transfer from the phenol radical cation to the base, step 3 in Scheme 3b. In MeCN, 2,4,6-tri-*tert*-butylphenol radical cation has a pK_a of ca. 0⁶⁰ and protonated benzylamine has a pK_a of 17,³⁸ yielding a ΔpK_a of 17. This provides a crude prediction of a shift of 1 V ($\Delta E = 0.059 \text{ V} \times \Delta pK_a$), somewhat larger than the observed 0.73 V difference between $E(\text{•ArO-NH}_3^+/\text{HOAr-NH}_2)$ vs $E(\text{•Bu}_3\text{ArOH}^{+0})$.

2. Mechanistic Analysis. There are three reasonable mechanisms for the one-electron oxidation of the hydrogen-bonded phenols (Scheme 4). Rate-limiting outer-sphere electron transfer could yield the phenolic radical cation (**•HOAr-B**), which would be followed by fast proton transfer to give the product (ET1–PT1). Radical cations of simple phenols are well-established transients, particularly in photochemical processes.⁶¹ Alternatively, pre-equilibrium proton transfer to yield the zwitterion (**•OAr-BH⁺**) could be followed by electron transfer (PT2–ET2). Zwitterions such as **•OAr-BH⁺** are well known in phenol-base chemistry, particularly when the phenolic portion is highly acidic, as in *p*-nitrophenols.^{39,40,62} Rate-limiting proton transfer is ruled out because different oxidants react at different rates and because PT between electronegative elements in general occurs at very fast rates.⁶³ The defining characteristic of the stepwise mechanisms is the formation of an intermediate with a finite lifetime. The third mechanism is the concerted transfer of both particles, CPET, defined by the absence of an intermediate along the reaction coordinate. “Concerted” implies that both particles move in a single kinetic step but does not imply synchronous movement of the proton and electron.

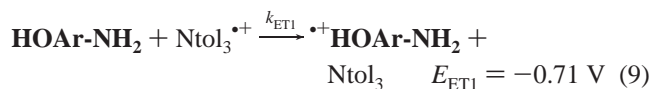
There are three experimental markers indicating the oxidation mechanism as CPET. First, isotope effects on the oxidation of **DOAr-ND₂** and **DOAr-py** (1.6–2.8 depending on oxidant and

- (54) March, J. *Advanced Organic Chemistry*, 4th ed.; Wiley: New York, 1992; p 76.
- (55) Kanamori, D.; Furukawa, A.; Okamura, T.; Yamamoto, H.; Ueyama, N. *Org. Biomol. Chem.* **2005**, *3*, 1453–1459.
- (56) For sterically encumbered phenols such as **•Bu₃ArOH**, hydrogen bonding to solvent is a small effect. For instance, 2,6-di-*tert*-butyl-4-methylphenol (BHT) is only 14% hydrogen-bonded in MeCN: Wren, J. J.; Lenthén, P. M. *J. Chem. Soc.* **1961**, 2557–2560.
- (57) Sjödin, M.; Styring, S.; Åkermark, B.; Sun, L.; Hammarström, L. *Philos. Trans. R. Soc. London B* **2002**, *357*, 1471–1479.
- (58) (a) Lucarini, M.; Pedulli, G. F.; Guerra, M. *Chem. Eur. J.* **2004**, *10*, 933–939. (b) Lucarini, M.; Mugnaini, V.; Pedulli, G. F.; Guerra, M. *J. Am. Chem. Soc.* **2003**, *125*, 8318–8329. (c) Amorati, R.; Lucarini, M.; Mugnaini, V.; Pedulli, G. F. *J. Org. Chem.* **2003**, *68*, 5198–5204. (d) DFT calculations suggest an H-bond strengthening of 8.6 kcal mol⁻¹ for 4-methoxy-1,8-naphthalenediol, but experimental results indicate that this is overestimated by as much as 2 kcal mol⁻¹. Foti, M. C.; Barclay, L. R. C.; Ingold, K. U. *J. Am. Chem. Soc.* **2002**, *124*, 12881–12888.
- (59) Hydrogen bond strengths have been shown to increase with decreasing difference in pK_a of the hydrogen bond donor and acceptor (ΔpK_a): Shan, S.-O.; Herschlag, D. *Proc. Natl. Acad. Sci. U.S.A.* **1996**, *93*, 14474–14479). This value is smaller in the phenol-amine ($pK_{a(\text{phenol})} - pK_{a(\text{amine})} \approx 27 - 17 = 10$, vs the radical cation $pK_{a(\text{PhOH}^+)} - pK_{a(\text{amine})} \approx 17 - 0 = 17$). The case is opposite for **HOAr-py**, where the relevant pK_a 's are 27 (PhOH), 12 (pyridine), and 0 (PhOH⁺) (MeCN pK_a data from refs 38 and 60).

- (60) (a) Reference 48a. (b) The difference between the phenol pK_a values in DMSO and MeCN is taken as 9.5 units according to the following: Chantooni, M. K., Jr.; Kolthoff, I. M. *J. Phys. Chem.* **1976**, *80*, 1306–1310.
- (61) (a) Brede, O.; Hermann, R.; Karakostas, N.; Naumov, S. *Phys. Chem. Chem. Phys.* **2004**, *6*, 5184–5188. (b) Ganapathi, M. R.; Hermann, R.; Naumov, S.; Brede, O. *Phys. Chem. Chem. Phys.* **2000**, *2*, 4947–4955.
- (62) (a) Rospenk, M.; Fritsch, J.; Zundel, G. *J. Phys. Chem.* **1984**, *88*, 321–323. (b) Koll, A.; Rospenk, M.; Sobczyk, L. *J. Chem. Soc., Faraday Trans. 1* **1981**, *77*, 2309–2314. (c) Rospenk, M. *J. Mol. Struct.* **1990**, *221*, 109–114.
- (63) Bell, R. P. *The Proton in Chemistry*; Cornell University Press: Ithaca, NY, 1973.

phenol) can only be explained through CPET. In rate-limiting electron transfer (ET1), no bond is made or broken in the ET step and, like other electron transfers,^{64a,65} there would be only a small secondary isotope effect. The proton-first pathway PT2–ET2 would have an equilibrium PT isotope effect, which would also be small.

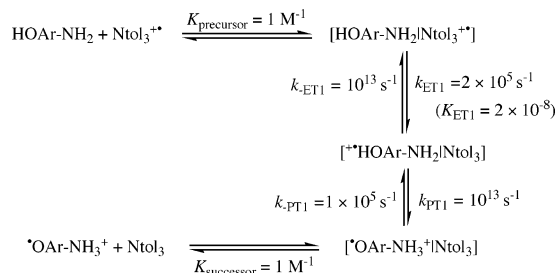
Second, the intermediates in the stepwise mechanisms appear to be too high in energy to be involved in the reactions. In the ET1–PT1 mechanism for **HOAr-NH₂** + [N(tol)₃]⁺, the ET1 step (eq 9) is estimated to have $E_{\text{ET1}} = -0.71$ V ($\Delta G_{\text{ET1}} = 16$ kcal mol⁻¹, $K_{\text{ET1}} = 10^{-12}$). This estimate uses $E(^+\text{HOAr-NH}_2/$



HOAr-NH₂) = 1.09 V, taken to be the same as $E(\text{Bu}_3\text{PhOH}^{+/0})$ ⁵³ and $E(\text{HOAr-OH}^{+/0})$ and 0.11 V below $E(\text{MeOAr-NH}_2^{+/0})$ (as noted above, hydrogen-bonding effects are likely to be small). The estimated value of ΔG_{ET1} is significantly higher than the observed Eyring barrier for this reaction, $\Delta G^\ddagger = 11$ kcal mol⁻¹ (from $k = 1.1 \times 10^5$ M⁻¹ s⁻¹ and the Eyring equation with $\kappa = 1$;⁵² with smaller prefactors or $\kappa < 1$ the discrepancy would be larger^{66,67}). For $\bullet^+\text{HOAr-NH}_2$ to be a viable intermediate (eq 9), our estimate of the potential would have to be in error by more than 0.2 V. (This would also predict a dependence on driving force different than what is observed, as described below.) This analysis can equivalently be framed in terms of rate constants instead of barriers. The values $K_{\text{ET1}} = k_{\text{ET1}}/k_{-\text{ET1}} = 10^{-12}$ (see above) and $k_{\text{ET1}} = k_{\text{obs}} = 10^5$ M⁻¹ s⁻¹ would imply an impossible $k_{-\text{ET1}} = 10^{17}$ M⁻¹ s⁻¹, much faster than the diffusion limit in MeCN.⁶⁸ Similar arguments hold for the **HOAr-py** and **HOAr-im** systems.

A more complete analysis of the ET1–PT1 pathway includes precursor and successor complexes, as illustrated for the **HOAr-NH₂** + [N(tol)₃]⁺ reaction in Scheme 5. The formation of the precursor and successor complexes is assumed to have equi-

Scheme 5. Putative Kinetic Scheme for ET–PT Involving Precursor and Successor Complexes, Assuming $K_{\text{precursor}} = K_{\text{successor}} = 1$ M⁻¹ and $k_{-\text{ET1}} = k_{\text{PT1}} = 10^{13}$ s⁻¹ as the Best-Case Scenario



librium constants $K_{\text{precursor}} = K_{\text{successor}} = 1$ M⁻¹, as is commonly done.⁶⁷ No evidence for a precursor or successor complex is evident in optical spectra of reaction mixtures. The ET1 step generates the successor complex in which the proton has not transferred, [$\bullet^+\text{HOAr-NH}_2|\text{Ntol}_3$]. In the scenario most favorable to the ET1–PT1 pathway, this intermediate partitions equally between back electron transfer to the precursor complex ($k_{-\text{ET1}}$) and forward proton transfer (k_{PT1}) to [$\bullet^+\text{OAr-NH}_3^+|\text{Ntol}_3$], with both occurring at the fastest possible rate, $\sim 10^{13}$ s⁻¹. With these assumptions, k_{ET1} would have to be 2×10^5 M⁻¹ s⁻¹, based on the experimentally observed $k_{\text{obs}} = 1 \times 10^5$ M⁻¹ s⁻¹ and $K_5 = 2$ (eq 5, above). This requires K_{ET1} for ET within the precursor complex ($k_{\text{ET1}}/k_{-\text{ET1}}$) to be 2×10^{-8} , more than 10^4 larger than the K_{ET1} based on the estimated redox potentials (see above). And even in this best-case scenario, [$\bullet^+\text{HOAr-NH}_2|\text{Ntol}_3$] is barely an intermediate, since the 10^{13} s⁻¹ rate constants imply a half-life of only 35 fs, roughly one vibrational period for a 1000 cm⁻¹ mode. The reaction with [N(*p*-C₆H₄OCH₃)₃]⁺ provides even tighter constraints, because ET1 becomes an additional 0.22 V uphill (K_{ET1} is less favorable by 5×10^{-3}), but k_{obs} only changes by 10^{-2} . The constraints on K_{ET1} are also more stringent if the back electron or proton transfers have any barrier and are slower than the maximal 10^{13} s⁻¹.

It should be added that the most recent computational and experimental reports conclude that similar intermolecularly hydrogen-bonded [PhOH|base]⁺ species are not minima in the gas phase (proton transfer from O to the base proceeds without barrier).⁶⁹ If this is also the case for the solution **ArOH-B**⁺ species discussed here, they cannot, by definition, be intermediates.

The PT2–ET2 pathway is also very unlikely, based on thermochemical arguments similar to those above. The rate constant for PT2–ET2 is the product of the equilibrium constant for initial proton transfer (K_{PT2} , eq 1, above) and the ET rate constant from the zwitterion (k_{ET2} , eq 10). K_{PT2} might be



expected to be $\sim 10^{-9}$ on the basis of the difference in $\text{p}K_{\text{a}}$ of amines (~ 18) and phenols (~ 27) in MeCN.³⁸ Since this ignores potential electrostatic interactions in the zwitterion, we instead

- (64) Ebersson, L. *Electron Transfer Reactions in Organic Chemistry*; Springer-Verlag: New York, 1987; (a) pp 77–79, (b) pp 51–52, (c) p 27, and (d) pp 30–34 (using the radii in ref 71).
- (65) (a) Buhks, E.; Bixon, M.; Jortner, J. *J. Phys. Chem.* **1981**, *85*, 3763. (b) Smaller secondary isotope effects have been observed for related electron transfers, e.g. Gould, I. R.; Farid, S. *J. Am. Chem. Soc.* **1988**, *110*, 7883–5.
- (66) Pre-exponential factors from 10^{11} to 10^{13} M⁻¹ s⁻¹ have been used for bimolecular adiabatic electron transfer reactions, values described as a collision frequency or a rate of crossing at the transition state^{64,66a,67} (at 298 K, the Eyring prefactor $k_{\text{B}}T/h$ is 6×10^{12} s⁻¹). One recent paper^{66a} describes the choice of prefactor as related to whether solvent or inner-sphere motions are dominant in the reorganization energy, a level of detail that is not yet available for CPET processes. In this mechanistic section, the analysis uses the Eyring equation as is typical in mechanistic chemistry; in the Marcus theory section that follows, the most typical⁶⁷ $Z = 10^{11}$ M⁻¹ s⁻¹ is used. Using $Z = 10^{11}$ M⁻¹ s⁻¹ in this mechanistic context would give $\Delta G_{\text{ET1}}^{\ddagger} = 8$ kcal mol⁻¹ and would strengthen the argument against the PT1–ET1 mechanism; the estimate of ΔG_{ET1} would have to be off by more than 0.3 V. Thus, the use of the Eyring equation here is a conservative (worst-case) choice for this argument. (a) Hamann, T. W.; Gstrein, F.; Brunschwig, B. S.; Lewis, N. S. *J. Am. Chem. Soc.* **2005**, *127*, 13949–13954.
- (67) The Marcus equation is often applied to bimolecular reactions using 10^{11} M⁻¹ s⁻¹ as the prefactor (rather than the Eyring $k_{\text{B}}T/h$): $k = (10^{11} \text{ M}^{-1} \text{ s}^{-1}) \exp(-\Delta G^\ddagger/RT)^{67a-d}$; K_{P} is typically assumed to be ~ 1 M⁻¹, with work terms added where appropriate.^{67a-d,71} (a) Marcus, R. A.; Sutin, N. *Biochim. Biophys. Acta* **1985**, *811*, 265–322. (b) Sutin, N. *Prog. Inorg. Chem.* **1983**, *30*, 441–499. (c) Sutin, N. *Acc. Chem. Res.* **1982**, *15*, 275–282. (d) Nelsen, S. F.; Pladziewicz, J. R. *Acc. Chem. Res.* **2002**, *35*, 247–254.
- (68) Cf.: (a) McClelland, R. A.; Kanagasabapathy, J. V. M.; Banait, N. S.; Steenken, S. *J. Am. Chem. Soc.* **1992**, *114*, 1816–1823. (b) de Carvalho, I. M. M.; Gehlen, M. H. *J. Photochem. Photobiol. A: Chem.* **1999**, *122*, 109–113. (c) Kikuchi, K.; Sato, C.; Watabe, M.; Ikeda, H.; Takahashi, Y.; Miyashi, T. *J. Am. Chem. Soc.* **1993**, *115*, 5180–5184.

- (69) (a) Fang, Y.; Liu, L.; Feng, Y.; Li, X.; Guo, Q. *J. Phys. Chem. A* **2002**, *106*, 4669–4678. (b) Feng, Y.; Liu, L.; Fang, Y.; Guo, Q. *J. Phys. Chem. A* **2002**, *106*, 11518–11525. (c) Wang, Y.; Eriksson, L. A. *Int. J. Quantum Chem.* **2001**, *83*, 220–229. (d) O'Malley, P. J. *J. Am. Chem. Soc.* **1998**, *120*, 11732–11737. (e) Kim, H.; Green, R. J.; Qian, J.; Anderson, S. L. *J. Chem. Phys.* **2000**, *112*, 5717–5721. (f) A minimum for a [**HOAr-im**]⁺ species in solution has been calculated in ref 30b.

use the more conservative experimental value, $K_{PT2} < 10^{-4}$, derived from UV–vis spectra (see above). The value $k_{obs} > 10^7 \text{ M}^{-1} \text{ s}^{-1}$ for $\text{HOAr-NH}_2 + [\text{N}(p\text{-C}_6\text{H}_4\text{Br})_3]^+$ then implies $k_{ET2} > 10^{11}$, faster than the diffusion limit in MeCN.⁶⁸ An analogous argument can be made with barrier heights and with precursor and successor complexes.

The third argument for the CPET mechanism is the dependence of barrier on driving force. For $\text{HOAr-NH}_2 + [\text{NAr}_3]^+$, a plot of $\Delta\Delta G^\ddagger$ vs $\Delta\Delta G^\circ$ has a slope 0.53 [$\Delta\Delta G^\circ = nF(E_1 - E_n)$ and $\Delta\Delta G^\ddagger = RT \ln(k_1/k_n)$]. Following the discussion above, the stepwise path with rate-limiting ET1 would require $\Delta G^\ddagger_{ET1} \approx \Delta G^\circ_{ET1}$ and therefore that $\Delta\Delta G^\ddagger/\Delta\Delta G^\circ \approx 1$ ($\Delta G^\circ \approx \lambda$ in the Marcus picture; see below).⁶⁷ The initial PT2 mechanism requires that $\Delta G^\ddagger_{ET2} \approx 0$, so $\Delta\Delta G^\ddagger/\Delta\Delta G^\circ \approx 0$ ($-\Delta G^\circ \approx \lambda$). As discussed in the next section, $\Delta\Delta G^\ddagger/\Delta\Delta G^\circ = 0.53$ is close to the value of 0.5 predicted by Marcus theory for the concerted process in this $|\Delta G^\circ_{CPET}| \ll 2\lambda$ situation. The dependence of barrier on driving force has previously been used by Okamura et al. to discuss stepwise vs concerted PCET pathways.²⁰

In sum, the isotope effects, the thermochemistry, and the dependence of the rate constants on driving force are consistent only with a concerted mechanism. These conclusions are consistent with the findings of Linschitz, Hammarström, and Nocera, who have all found CPET mechanisms for their systems, which include both aqueous and nonaqueous media.^{7–9}

3. Analysis Using Marcus Theory. From one perspective, the phenol–bases **HOAr-B** are simply outer-sphere electron transfer reagents, so Marcus theory may be appropriate to analyze these reactions. However, the inner-sphere reorganizations for **HOAr-B/OAr-BH⁺** are unusual because they involve not only small shifts in equilibrium bond distances, as in the standard Marcus picture, but also movement of a proton across an $\text{OH}\cdots\text{N}$ hydrogen bond. The proton can be thought of as transferring $\sim 0.7 \text{ \AA}$ between two minima on an adiabatic potential energy surface.⁷⁰ This would not seem to fit easily into the standard Marcus model, where a single parabolic surface, defined by the reorganization energy λ , describes all of the solvent and inner-sphere reorganizations. Current, more refined theoretical formulations of CPET treat the proton transfer explicitly but are more complicated and require more parameters than are readily determined experimentally.²³ So, despite its simplifications, the adiabatic Marcus equation is still the logical

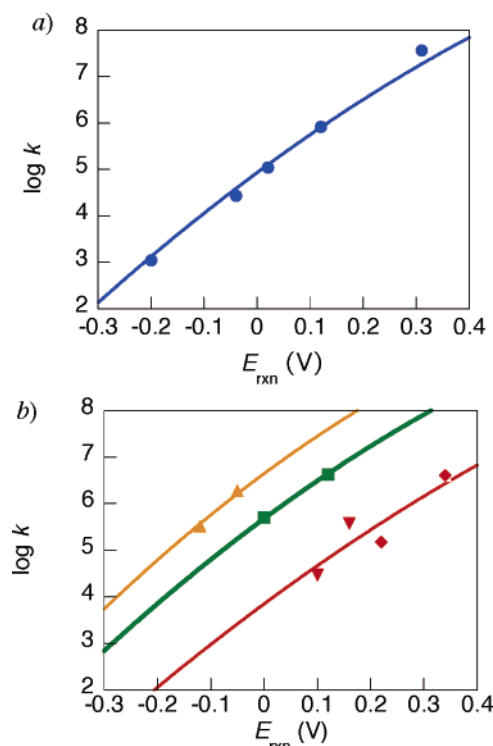


Figure 6. $\log(k)$ vs E_{rxn} for oxidations (a) of **HOAr-NH₂** by $[\text{NAr}_3]^+$ (●) and (b) of **HOAr-py** by $[\text{Fe}(\text{Me}_3\text{phen})_3]^{3+}$ (▲) and $[\text{Fe}(\text{R}_2\text{bpy})_3]^{3+}$ (■) and **HOAr-NH₂** by $[\text{Fe}(\text{Me}_3\text{phen})_3]^{3+}$ (▼) and $[\text{Fe}(\text{R}_2\text{bpy})_3]^{3+}$ (◆). The curves are fits to eq 12.

starting point because it predicts barriers and rate constants using only the two parameters λ and ΔG° (eqs 11 and 12).^{67,71}

$$\Delta G^\ddagger = \frac{\lambda}{4} \left(1 + \frac{\Delta G^\circ}{\lambda} \right)^2 \quad (11)$$

$$k = [10^{11} \text{ M}^{-1} \text{ s}^{-1}] e^{-\frac{\lambda}{4RT} \left[1 + \left(\frac{\Delta G^\circ}{\lambda} \right)^2 \right]} \quad (12)$$

$$\lambda_{12} = \frac{1}{2} (\lambda_{11} + \lambda_{22}) \quad (13)$$

The kinetic and thermochemical data for **HOAr-B** + oxidant reactions (Table 3) can be fit by eq 12, as shown in Figure 6.⁷² The data sets are also well fit by straight lines; as noted above, the slope $\Delta\Delta G^\ddagger/\Delta\Delta G^\circ$ for the **HOAr-NH₂** + $[\text{NAr}_3]^+$ reactions is 0.53. The limited range of experimentally accessible driving forces (0.51 V) does not provide a test of the predicted parabolic dependence of $\log(k)$ on E_{CPET} .

The reorganization energies for the oxidations of **HOAr-NH₂** derived from eq 12 are $34 \pm 1 \text{ kcal mol}^{-1}$ (1.5 eV) for the reactions with $[\text{NAr}_3]^+$, $38 \pm 2 \text{ kcal mol}^{-1}$ (1.9 eV) for the reactions with $[\text{Fe}(\text{N-N})_3]^{3+}$ (N–N = R₂bpy, Me₃phen), and $35 \pm 1 \text{ kcal mol}^{-1}$ (1.5 eV) from the single rate constant oxidation by 10-methylphenothiazinium (MPT⁺) (Table 4). Following the additivity postulate (eq 13), each of these cross reaction values (λ_{12}) is the average of the λ 's for the individual self-exchange reactions $\text{A}^+ + \text{A} \rightarrow \text{A} + \text{A}^+$. The λ_{11} for N(tol)₃/ $[\text{N}(\text{tol})_3]^{3+}$ self-exchange in MeCN is 12 kcal mol^{-1} (0.5 eV),⁴³ which is taken as characteristic of the series of NAr_3^+ oxidants used here. λ_{11} for MPT^{+/0} is similar (9 kcal mol^{-1} , 0.4 eV);⁷³ that for $[\text{Fe}(\text{bpy})_3]^{3+/2+}$ in MeCN is twice as large (24 kcal mol^{-1} , 1.0 eV).⁷⁴ Using eq 13, these values yield reorganization energies for **HOAr-NH₂/OAr-NH₃⁺** self-exchange of 53 ± 3 ,

(70) (a) O \cdots N distances in these and related structures are in the range 2.53–2.65 Å.³³ With typical O–H and N–H distances of 0.96 and 1.01 Å,^{70a} the distance between proton positions in OH \cdots N vs O \cdots HN tautomers should be 0.56–0.68 Å in a linear hydrogen bond. In the bent structures likely for **HOAr-B**, the distances should be ~ 0.7 – 0.8 \AA . (b) *CRC Handbook of Chemistry and Physics*, 54th ed.; Weast, R. C., Ed.; CRC Press: Cleveland, OH, 1973; pp F198–F199.

(71) (a) An electrostatic correction to ΔG° for the Marcus analysis^{64c} has been included for the **HOAr-B** + $[\text{Fe}(\text{N-N})_3]^{3+}$ reactions: $\Delta G^{\circ'} - \Delta G^\circ = (Z_1 - Z_2 - 1)(331.2f)/(Dr_{12}) = 0.76 \text{ kcal mol}^{-1}$, or 0.03 eV; $Z_1 = 0$; $Z_2 = +3$; $f = 0.60$ (for 0.1 M ionic strength);^{64c} $D = 37.5$; $r_{12} = 13.9 \text{ \AA}$. The radius of **HOAr-B** was calculated from the lowest crystallographic volume $\sim 1400 \text{ \AA}^3$ and $V = (4/3)\pi r^3$, yielding $r = 6.9 \text{ \AA}$. The radius of $[\text{Fe}(\text{bpy})_3]^{3+}$ is assumed to be 7.0 Å.^{71b} For the **HOAr-B** + $[\text{NAr}_3]^+$ reactions, one of the species on each side of the equation is uncharged; therefore, the correction is zero. (b) Schlesener, C. J.; Amatore, C.; Kochi, J. K. *J. Am. Chem. Soc.* **1984**, *106*, 3567–3577.

(72) Fitting of k vs T data to eqs 12 and 15 implicitly assumes that λ is constant with temperature. For λ to change significantly over such a small temperature range (30–50 K) would require λ to have a very large entropic component ($\Delta\lambda = \Delta[\Delta H_2^\ddagger] - \Delta[T\Delta S_2^\ddagger] \approx \Delta T[\Delta S_2^\ddagger]$, which would be $\leq 1 \text{ kcal mol}^{-1}$, even if ΔS_2^\ddagger were $20 \text{ cal K}^{-1} \text{ mol}^{-1}$).

Table 4. Activation Parameters, Adiabatic Reorganization Energies, and Apparent Non-adiabatic Reorganization Energies and H_{rp} Values for Phenol–Base Oxidations^a

reaction	$\lambda_{12}(E)^b$	$\lambda_{12}(T)^b$	λ_{11}^c	$[\lambda_{12}(\text{non-ad})]^d$	$[H_{\text{rp}}]^d$	ΔH^\ddagger ^e	ΔS^\ddagger ^e
HOAr-NH₂ + [N(Ar) ₃] ^{•+} ^f	34 ± 1	33 ± 1	53 ± 3	[29.6 ± 1.6]	[10 ± 4]	6.3 ± 0.4	−14.1 ± 1.3
HOAr-NH₂ + [Fe(N–N) ₃] ³⁺ ^g	38 ± 2	<i>h</i>	52 ± 4	<i>h</i>	<i>h</i>	<i>h</i>	<i>h</i>
HOAr-NH₂ + [MPT] ^{•+}	35 ± 1 ⁱ	<i>h</i>	58 ± 3 ⁱ	<i>h</i>	<i>h</i>	<i>h</i>	<i>h</i>
HOAr-py + [Fe(R ₂ bpy) ₃] ³⁺ ^{g,j}	27 ± 1	27 ± 1	30 ± 3	[23.2 ± 1.6]	[6 ± 2]	4.7 ± 0.4	−16.0 ± 1.2
HOAr-py + [Fe(Me _x phen) ₃] ³⁺ ^g	22 ± 1	<i>h</i>	23 ± 3	<i>h</i>	<i>h</i>	<i>h</i>	<i>h</i>
HOAr-im + [N(anisyl) ₃] ^{•+} ^k	25 ± 2 ⁱ	25 ± 2	36 ± 4 ⁱ	[17 ± 3]	[4 ± 3]	7.0 ± 0.7	−17 ± 3

^a ΔH^\ddagger and λ in kcal mol^{−1}, ΔS^\ddagger in cal K^{−1} mol^{−1} (eu), and H_{rp} in cm^{−1}. ^b $\lambda_{12}(E)$ and $\lambda_{12}(T)$ are the adiabatic reorganization energies calculated from the dependence of k on either E° or T using eq 12 (Figures 5 and 6). ^c λ_{11} is the adiabatic reorganization energy for **HOAr-B[•]OAr-HB^{•+}** self-exchange from eq 13 [using the average of $\lambda_{12}(E)$ and $\lambda_{12}(T)$]. ^d $\lambda_{12}(\text{non-adiabatic})$ and H_{rp} from eq 15, which may not be appropriate; see text. ^e Determined by fitting k_{obs} vs T data (Figure 5) to the Eyring equation.⁵² ^f Temperature-dependent results for **HOAr-NH₂** + [N(tol)₃]^{•+}, 280 ≤ T ≤ 327 K. ^g Corrected for work terms following refs 64 and 71. ^h Not determined. ⁱ From a single phenol–oxidant pair. ^j Temperature-dependent results for **HOAr-py** + [Fe(Me₂bpy)₃]³⁺, 279 ≤ T ≤ 318 K. ^k Anisyl = −C₆H₄OMe; 279 ≤ T ≤ 309 K.

53 ± 4, and 58 ± 3 kcal mol^{−1} (2.4 ± 0.2 eV). These are the same within experimental error, which is an indication that it is appropriate to use the adiabatic Marcus equation to analyze these reactions. The single rate constant for **HOAr-im** + [N(*p*-C₆H₄OMe)₃]^{•+} gives $\lambda_{11} = 36 \pm 3$ kcal mol^{−1} (1.4 eV) for CPET self-exchange.

The rate constants for oxidation of **HOAr-py** fall on different lines for oxidants [Fe(R₂bpy)₃]³⁺ (R = H, Me) vs [Fe(Me_xphen)₃]³⁺ (Me_x = 4,7-Me₂, 3,4,7,8-Me₄). The λ_{12} values are 27 ± 1 kcal mol^{−1} (R₂bpy oxidants) and 22 ± 1 kcal mol^{−1} (Me_xphen oxidants). The distinction is surprising because of the similarity of these oxidants. The self-exchange rate constants for these species are similar, with the phenanthroline derivatives reacting ca. 3 times faster, although this comparison is complicated by scatter among the different derivatives, counterion and ionic strength effects, etc.^{1c} Taking $\lambda_{11} \cong 24$ and 21 kcal mol^{−1} for [Fe(R₂bpy)₃]^{3+/2+} and [Fe(Me_xphen)₃]^{3+/2+}, respectively, yields apparent $\lambda_{11}(\text{HOAr-py})$ values of 30 ± 3 and 23 ± 3 kcal mol^{−1} for the different oxidants. These values are different, as indicated by the distinct lines in Figure 6. This discrepancy suggests a deviation from the adiabatic Marcus treatment, perhaps due to non-adiabaticity or to ion-pairing issues, as will be probed in future work.⁷⁵ The oxidations of **HOAr-NH₂** do not show such a distinction between reactions with [Fe(R₂bpy)₃]³⁺ vs [Fe(Me_xphen)₃]³⁺, although there is some scatter in the rate constants (bottom curve of Figure 6b). Fitting these rate constants separately yields cross reaction λ_{12} and **HOAr-NH₂** self-exchange λ_{11} values that agree within error: [Fe(R₂bpy)₃]³⁺, $\lambda_{12} = 39 \pm 2$, $\lambda_{11} = 53 \pm 4$; [Fe(Me_xphen)₃]³⁺, $\lambda_{12} = 37 \pm 2$, $\lambda_{11} = 53 \pm 4$ kcal mol^{−1}.

Reorganization energies can also be derived from the temperature dependence of the rate constants using eq 12.⁷⁶ These are given as $\lambda_{12}(T)$ in Table 4, to distinguish them from the reorganization energies derived from the dependence on E_{CPET} , $\lambda_{12}(E)$. The $\lambda_{12}(E)$ and $\lambda_{12}(T)$ values are the same within experimental error for the three cases where comparisons are

made. This agreement, between two different kinds of analysis and involving mostly independent data sets, supports the use of the Marcus equation for these CPET reactions. Another correct prediction of the Marcus treatment is that $\Delta\Delta G^\ddagger/\Delta\Delta G^\circ = 0.5 + \Delta G^\circ/2\lambda$. Using the values in Tables 3 and 4 for the five **HOAr-NH₂** + NAr₃^{•+} reactions, $0.5 + \Delta G^\circ/2\lambda$ ranges from 0.39 to 0.57, with an average value of 0.49. This is in good agreement with the experimental linear fit, $\Delta\Delta G^\ddagger/\Delta\Delta G^\circ = 0.53$.

The electrochemical rate constant k_{el} provides an additional test of the applicability of the adiabatic Marcus treatment. While rigorous comparison of heterogeneous and homogeneous electron transfer kinetics is complex, there is often a good correspondence between k_{el} and the homogeneous self-exchange rate constant k_{11} , via eq 14.^{44a,77} Equation 14 follows from the

$$\sqrt{\frac{k_{11}}{10^{11} \text{ M}^{-1} \text{ s}^{-1}}} = \frac{k_{\text{el}}}{10^4 \text{ cm}^{-1} \text{ s}^{-1}} \quad (14)$$

assumption that a given reagent has similar intrinsic barriers for homogeneous and heterogeneous electron transfer. The rate constants are divided by the different collision frequencies, and the self-exchange k_{11} appears as a square root because it involves two molecules and therefore two intrinsic barriers. k_{11} for **HOAr-NH₂** has not been directly determined but is calculated to be 8 M^{−1} s^{−1} using the adiabatic Marcus equation (eq 12) with $\lambda_{11} = 55$ kcal mol^{−1} (the average of the three experimentally derived values in Table 4). Then $(k_{11}/10^{11})^{1/2} = 9 \times 10^{-6}$, a factor of 20 larger than $(k_{\text{el}}/10^4) = 3 \times 10^{-7}$. This is good agreement given the approximate nature of eq 14 and that the k_{el} of 3×10^{-3} cm s^{−1} lies on the cusp of the conditions where eq 14 holds — according to Swaddle, only for $k_{\text{el}} \leq 10^{-2}$ cm s^{−1}.^{77b}

The results reported here are among the first confirmations that the adiabatic Marcus equation is applicable to this class of CPET reactions, in which the proton and electron are clearly separated in the reactants or products. We and others have used Marcus theory for CPET reactions, assuming its applicability.^{8,24} The tests described here are the equivalence of the intrinsic barriers derived from the dependence on driving force, from the dependence on temperature, and from different reagents, and the agreement between electrochemical and solution rate constants. It should be noted that these tests are not especially stringent and that there is the possibility of a deviation in the difference λ 's derived for **HOAr-py** with the different iron oxidants, which will be explored in more detail in future work.⁷⁵ Hammarström and co-workers have previously shown that

(73) Kowert, B. A.; Marcoux, L.; Bard, A. J. *J. Am. Chem. Soc.* **1972**, *94*, 5538–5550.

(74) (a) $\lambda_{22}(\text{[Fe(bpy)}_3\text{]}^{3+})$ was calculated from the self-exchange rate^{1c} using the adiabatic Marcus equation with $Z = 10^{11}$, taking $\lambda = 0.25\Delta G^\ddagger_{11}$ and a [Fe(bpy)₃]³⁺ self-exchange rate. The self-exchange rate for [Fe(4,4'-Me₂-bpy)₃]³⁺ is 2 times faster than that for the bpy derivative,^{1c} so it is likely that [Fe(5,5'-Me₂-bpy)₃]³⁺ would also be slightly faster.

(75) Markle, T. F.; Rhile, I. J.; Nagao, H.; DiPasquale, A. G.; Mayer J. M., manuscript in preparation and work in progress.

(76) The calculation of an adiabatic λ from the temperature-dependent rate data assumes that the equilibrium constants for formation of the precursor and successor complexes are 1 M^{−1} at all temperatures; see, however, the discussion of non-adiabatic character below.

(77) (a) Marcus, R. A. *J. Phys. Chem.* **1963**, *67*, 853–857. (b) Fu, Y.; Swaddle, T. W. *J. Am. Chem. Soc.* **1997**, *119*, 7137–7144.

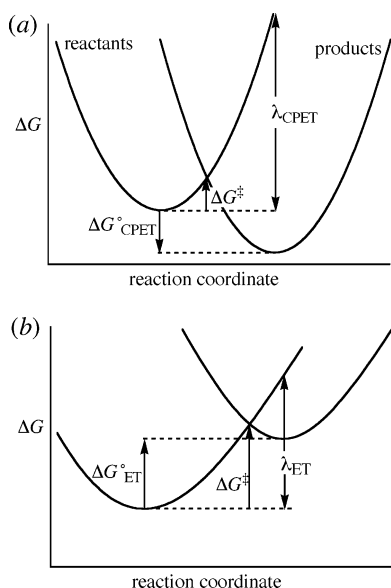


Figure 7. Marcus potential energy surfaces for (a) CPET, with a favorable $\Delta G^\circ_{\text{CPET}}$ but a large λ_{CPET} , in contrast to (b) initial ET (to be followed by PT), with an unfavorable $\Delta G^\circ_{\text{ET}}$ but a smaller λ_{ET} .

similar λ 's are derived from driving force and temperature-dependent measurements.⁸

The 56 kcal mol⁻¹ (2.4 eV) reorganization energy for **HOAr-NH₂**•**OAr-NH₃⁺** self-exchange in MeCN is quite a large value.^{64b,67d} **HOAr-NH₂** is fairly close in size to N(tol)₃ and has the same charge, yet the phenol-amine CPET λ_{11} is 4.7 times that of the triarylamine: 56 vs 12 kcal mol⁻¹. The 12 kcal mol⁻¹ value for N(tol)₃/[N(tol)₃]^{•+} is typical of λ 's for outersphere electron transfer by aromatic organic molecules, usually ≤ 20 kcal mol⁻¹.^{64b} **HOAr-NH₂** has a much higher intrinsic barrier because ET is coupled to transfer of the proton. Hammarström and co-workers have reached the same conclusion in their studies, that CPET oxidations of tethered phenol and indole groups in water have much higher intrinsic barriers than the pure electron transfers from the same reagents.⁸ The similarities of our conclusions are striking in light of the differences in our systems, Hammarström measuring rate constants in water for intramolecular ET coupled to proton transfer to the bulk aqueous solution. The λ_{11} 's for **HOAr-im** and **HOAr-py** are smaller than that of **HOAr-NH₂** but still larger than those for aromatic organic molecules. The significant differences in intrinsic barriers for the amino vs the pyridyl and imidazolyl derivatives will be discussed in a future report.⁷⁵

The large intrinsic barriers to CPET — indicating that it is inherently difficult — would suggest that this concerted reaction would be disfavored relative to the stepwise ET-PT mechanism. If the driving forces for the competing rate-limiting steps were identical, this would indeed be the case. However, in this system $E^\circ(\text{CPET})$ is substantially more favorable than $E^\circ(\text{initial ET})$, which leads to the lower barrier for the CPET (Figure 7). In

other words, initial pure ET or PT is disfavored because of the high energy of the intermediate that would be formed. A similar argument has been advanced by Hammarström et al. for aqueous CPET reactions.⁸

Extrapolation of these conclusions to a specific biological system requires caution because typically the driving forces for CPET, pure ET, and pure PT are not known. The local dielectric constant and nearby protein residues can substantially affect these values (and the intrinsic barriers). When initial ET or PT is energetically competitive with CPET, as found for instance for quinone reductions in PS I, stepwise pathways are favored.²⁰ However, the concerted mechanism likely occurs in many situations when pure ET and pure PT are high in energy.

4. Adiabatic vs Non-adiabatic Electron Transfer. The discussion above has utilized the adiabatic Marcus equation, but many electron transfer reactions are non-adiabatic. Current theoretical descriptions of CPET use non-adiabatic formalisms.²³ In a non-adiabatic reaction, there is a low probability of crossing from the reactant to product diabatic surfaces when the system reaches the transition structure (transmission coefficient $\kappa \ll 1$). In adiabatic reactions, the system is well described by a ground-state potential energy surface with $\kappa \approx 1$. The matrix element H_{rp} is a measure of the interaction of the surfaces and appears in the pre-exponential of the non-adiabatic Marcus equation (eq 15). Values of H_{rp} less than ~ 200 cm⁻¹ ($\sim k_{\text{B}}T$) normally indicate a non-adiabatic reaction.⁷⁸

$k =$

$$K_{\text{p}} \frac{4\pi^2 H_{\text{rp}}^2}{h\sqrt{4\pi[\lambda(\text{non-ad})]k_{\text{B}}T}} e^{-\{[\lambda(\text{non-ad})+\Delta G^\circ]^2/4[\lambda(\text{non-ad})]k_{\text{B}}T\}} \quad (15)$$

H_{rp} is best determined through measurements in the region where $-\Delta G^\circ \cong \lambda$, but such measurements are not possible with this system. An alternative though problematic approach fits k as a function of T to eq 15, to obtain H_{rp} and the non-adiabatic reorganization energy $\lambda_{12}(\text{non-ad})$.⁷² This analysis requires the assumption that the equilibrium constants for forming the precursor complexes K_{p} are 1 at all temperatures, in the absence of electrostatic work (note ΔG° has been found to be roughly constant with temperature). The apparent values for H_{rp} , 10 ± 4 , 6 ± 2 , and 4 ± 3 cm⁻¹, and $\lambda_{12}(\text{non-ad})$ are given in Table 4. These H_{rp} values would normally indicate a non-adiabatic reaction. However, K_{p} is likely to be smaller than 1 (two standard estimating approaches give $K_{\text{p}} \cong 0.86$ ^{64d} and 0.02⁷⁹) and is likely to have a temperature dependence, becoming smaller at higher temperatures due to an unfavorable entropy. Including either $K_{\text{p}} < 1$ or such a temperature dependence would increase the value of H_{rp} . Thus, the apparent H_{rp} values calculated from eq 15 with $K_{\text{p}} = 1$ are lower limits.⁸⁰ For instance, if the entropy of forming the precursor complex, $\Delta S^\circ_{\text{p}}$, were -10 cal K⁻¹ mol⁻¹ and $K_{\text{p}} = 0.02$ at 298 K, the derived H_{rp} would be 130 cm⁻¹.⁸¹

In sum, the CPET reactions described here appear to be at most mildly non-adiabatic. The slowness of the electron transfer reactions of **HOAr-NH₂** is due not to substantial non-adiabatic character but rather to large reorganization energies. For example, **HOAr-NH₂** + [N(tol)₃]^{•+} is $\sim 10^5$ slower than [N(tol)₃]^{•+/0} self-exchange; both processes have $\Delta G^\circ \cong 0$. This is because λ_{12} for **HOAr-NH₂** + [N(tol)₃]^{•+} is substantially

(78) Newton, M. D.; Sutin, N. *Annu. Rev. Phys. Chem.* **1984**, *35*, 437–480 (esp. p 451).

(79) Sutin, N. *Prog. Inorg. Chem.* **1983**, *30*, 441–498.

(80) The Eyring parameters for these reactions (Table 4) also suggest adiabatic processes. Non-adiabatic reactions should be marked by large negative ΔS^\ddagger to reflect the low probability of reaction, but the values observed, -14 to -17 eu, are modest for a bimolecular process.

(81) $K_{\text{p}} = 0.1$ (at 298 K) and $\Delta S_{\text{p}} = -10$ eu imply $\Delta H_{\text{p}} = -1.6$ kcal mol⁻¹. Using these assumptions, estimated values of H_{rp} and λ can be derived by fitting k_{ET} (where $k_{\text{ET}} = k_{\text{obs}}/K_{\text{p}}$) vs T data to eq 15.

larger than the λ_{11} of 12 kcal mol⁻¹ for [N(tol)₃]⁺⁰ self-exchange,⁴³ whether one uses the adiabatic $\lambda_{12} = 34$ kcal mol⁻¹ (from eq 12) or the non-adiabatic $\lambda_{12}(\text{non-ad}) = 30$ kcal mol⁻¹ (from eq 15 with $K_P = 1$). **HOAr-py** and **HOAr-im** have intrinsic barriers that are also large but are smaller than that for **HOAr-NH₂**. The origin of these barriers and the differences among these structurally similar phenol–bases will be discussed in a future publication.⁷⁵

Conclusions

One-electron oxidation of phenols hydrogen-bonded to a pendant base, **HOAr-B**, yields radical cations in which the phenolic proton has transferred to the base, **•OAr-BH⁺**. Three cases are reported here, with amino, pyridyl, and imidazolyl bases. These systems serve as models for hydrogen-bonded tyrosine residues in proteins, and more generally as an archetype for a class of coupled proton–electron transfer reactions where the electron and proton travel to different sites. The redox potentials of these phenols are lower than those of simple phenols, reflecting the favorable transfer of the proton to the hydrogen-bonded base.

Reactions of **HOAr-B** with [NAr₃]⁺⁰ or [Fe(N–N)₃]³⁺ oxidants in MeCN follow simple bimolecular kinetics. The mechanism of oxidation involves concerted transfer of the proton and electron (CPET). Three arguments rule out the alternative stepwise mechanisms of initial proton and subsequent electron transfer, or initial electron and subsequent proton transfer. First, the primary kinetic isotope effects (1.6–2.8) are inconsistent with the stepwise pathways. Second, the rates of oxidation are too fast to involve the high-energy intermediates of the stepwise pathways (the observed barriers are lower than the estimated free energies of [**•OAr-BH⁺**] and [**•⁺HOAr-B**]). Third, the dependence of the rate on driving force for the reaction **HOAr-NH₂** + [NAr₃]⁺⁰, $\Delta\Delta G^\ddagger/\Delta\Delta G^\circ = 0.53$, is consistent only with the $|\Delta G^\circ| \ll 2\lambda$ situation found for CPET. Based on this work and related model systems,^{7–9} CPET is likely a common (albeit underappreciated) mechanism for phenol oxidations. It is favored when the phenol is hydrogen-bonded to a base and when the intermediates in the stepwise paths are high in energy. These conditions probably occur often in biological systems, although the local protein environment can have a substantial influence on the relevant energetics.

The CPET reactions are in general well described by the adiabatic Marcus equation (eq 12). Fitting the variation in k with E_{CPET} for a series of oxidants yields self-exchange reorganization energies $\lambda_{11} = 56 \pm 3$, 27 ± 4 , and 36 ± 3 kcal mol⁻¹ for **HOAr-NH₂•OAr-NH₃⁺**, **HOAr-py•OAr-pyH⁺**, and **HOAr-im•OAr-imH⁺**, respectively. For **HOAr-NH₂**, the same λ_{11} is found for three different oxidants, as required by the Marcus treatment. For each of the phenols, the temperature dependence of the rate constants gives the same λ_{11} as found from k vs E_{CPET} . The $\Delta\Delta G^\ddagger_{\text{CPET}}/\Delta\Delta G^\circ_{\text{CPET}} = 0.53$ for **HOAr-NH₂** + [NAr₃]⁺⁰ reactions is very close to the value of 0.5 predicted by the Marcus equation for this $|\Delta G^\circ_{\text{CPET}}| \ll 2\lambda$ case. The electrochemical rate constant for **HOAr-NH₂** correlates well with the calculated **HOAr-NH₂** self-exchange rate constant. These results support the use of simple Marcus theory for such CPET systems, although these are not particularly stringent tests.

A deviation from the adiabatic Marcus equation may have been observed in the different λ_{11} values obtained for oxidations of **HOAr-py** with [Fe(R₂bpy)₃]³⁺ (30 ± 3 kcal mol⁻¹) vs [Fe(Me_x-phen)₃]³⁺ (23 ± 3 kcal mol⁻¹).

The CPET rate constants are slower than the rate constants of pure ET reactions of comparable organic reagents, especially for **HOAr-NH₂**. This is a result of the large intrinsic barriers for CPET. A small part of this rate difference could be that the CPET reactions are more non-adiabatic, but the data do not support highly non-adiabatic CPET. The 27–56 kcal mol⁻¹ adiabatic reorganization energies for these reactions are significantly larger than typical λ 's for ET reactions of aromatic organic compounds. For instance, [N(tol)₃]⁺⁰ self-exchange has $\lambda_{11} = 12$ kcal mol⁻¹.⁴³ The pyridyl and imidazolyl compounds have significantly lower intrinsic barriers than the amino derivative. Future work will probe the origins of these barriers and the differences among the different phenols.⁷⁵

Experimental Section

General. Unless otherwise noted, reagents were purchased from Aldrich, solvents from Fischer, and deuterated solvents from Cambridge Isotope. MeCN was used as obtained from Burdick and Jackson (low-water brand) and stored in an argon-pressurized stainless steel drum plumbed directly into a glovebox. ⁿBu₄NPF₆ was recrystallized three times from EtOH and dried in vacuo for 2 days at 110 °C prior to use. ¹H NMR and ¹³C NMR spectra were recorded on Bruker AF300, AV300, AV301, DRX499, or AV500 spectrometers at ambient temperatures; chemical shifts are reported relative to TMS in ppm by referencing to the residual solvent signals. The UV–vis spectra were obtained on a Hewlett-Packard 8453 diode array spectrophotometer and are reported as λ_{max} in nm (ϵ , M⁻¹ cm⁻¹), except for the long-pathlength spectrum that was obtained on a CARY-500 instrument. The EPR spectrum was recorded on a Bruker EPX CW-EPR spectrometer operating at X-band frequency at room temperature.

The synthesis of **HOAr-NH₂**, equilibration experiments, crystallographic data, and the EPR spectrum of **•OAr-NH₃⁺** are given in the Supporting Information of this paper and of ref 24. Preparation of **MeOAr-NH₂** followed the procedure in Scheme 2, starting from the methyl bromoaryl ether C₆H₂(OMe)(2-Br)(4,6-Bu₂) (see Supporting Information). **HOAr-im** was prepared as described by Benivisy³⁰ by the condensation reaction: aldehyde + ammonium acetate + 4,4'-dimethoxybenzil. The preparation of **HOAr-py** used the Ni(dppe)₂ coupling of the phenol-derived Grignard and 2-bromopyridine described by Fujita,³¹ except with a BBr₃ deprotection of the methyl ether.⁸²

Electrochemistry. Cyclic voltammograms were taken on an E2 Epsilon electrochemical analyzer (Bioanalytical Systems) at ca. 5 mM substrate in anaerobic 0.1 M ⁿBu₄NPF₆/acetonitrile solution, unless otherwise specified. The electrodes were as follows: working, platinum disk (unless noted otherwise); auxiliary, platinum wire; and reference, Ag/AgNO₃ (0.01 M) in electrolyte solution. All potentials are reported vs a Cp₂Fe⁺⁰ internal standard. Errors are estimated to be ± 0.02 V. Representative CVs are included as Figure S17 of the Supporting Information.

For cyclic voltammetry at elevated and depressed temperatures, a single solution was used for each analyte. Typically, the electrochemical cell was prepared and degassed and CVs were collected, yielding $E_{1/2}$ vs Ag/AgNO₃. The entire cell was then placed in a warm water bath and allowed to come to thermal equilibrium before CVs were collected. This process was repeated using an ice bath. The cell was allowed to return to ambient temperature, and a final series of CVs were collected; in all cases, the $E_{1/2}$ was found to be within 5 mV of the initial room-temperature measurements. Last, ferrocene was added as an internal standard and another CV was obtained. The potential of ferrocene vs Ag/AgNO₃ was found to vary by less than 5 mV over the temperatures

(82) Zhang, H.; Kwong, F. Y.; Tian, Y.; Chan, K. S. *J. Org. Chem.* **1998**, *63*, 6886–6890.

studied, so room-temperature $\text{Cp}_2\text{Fe}^{+/0}$ was used as a reference for all of the CVs. A glassy carbon working electrode ($\phi = 3$ mm) was used for **HOAr-NH₂** and **HOAr-py** in these experiments. The driving force for the **HOAr-NH₂** + $[\text{N}(\text{tol})_3]^{+}$ and **HOAr-py** + $[\text{Fe}(\text{Me}_2\text{-bpy})_3]^{3+}$ reactions was taken as the difference of $E_{1/2}(\text{oxidant}) - E_{1/2}(\text{HOAr-B})$; see Table S21 in Supporting Information.

In the determination of the heterogeneous k_{el} for **HOAr-NH₂**, the platinum disk working electrode ($\phi = 1.6$ mm) was polished before each scan with commercial alumina solution and rinsed with water, dilute $\text{HNO}_3(\text{aq})$, ethanol, and acetonitrile before use. The uncompensated resistance R_u of the electrochemical cell was measured at each experiment and was found to be on the order of 500 Ω , which is expected to have a negligible effect on the measured potential E (<5 mV). Simulated CVs were produced with DigiSim version 3.03,⁴⁶ using the experimentally measured values for E_0 , E_{int} , E_{rev} , E_{end} , ν , electrode area (planar), D_{O} , D_{R} , and k_{el} . The mechanism model used was $\text{B} + e^- \rightarrow \text{A}$. The parameter α was taken to be 0.5.⁴⁵

Kinetics. Kinetics experiments were performed on an OLIS RSM-1000 stopped-flow apparatus in anaerobic MeCN. The data were analyzed with SpecFit global analysis software.⁵¹ Kinetics were fit to pseudo-first-order, second-order, or opposing second-order kinetics as appropriate. To determine the isotope effects, solutions were prepared

with a large excess of benchtop CH_3OD (1% v/v for **HOAr-NH₂** or 0.5% v/v for **HOAr-py**). Control experiments showed that aerobic addition of an equivalent amount of CH_3OH to MeCN solutions did not affect the rate. The isotope effects were corrected for the *OH* content in the CH_3OD (determined via ^1H NMR), 7% for the experiments with **DOAr-ND₂** and 4% for those with **DOAr-py**. Rate constants and data analyses are given in the Supporting Information of this paper and of ref 24.

X-ray crystallographic data and experimental descriptions are in the Supporting Information.

Acknowledgment. We gratefully acknowledge support from the U.S. National Institutes of Health (grant 2 R01 GM50422). Special thanks to Prof. Arnold Rheingold for crystallographic assistance with the **HOAr-py** crystal structure.

Supporting Information Available: Syntheses and cyclic voltammograms, and kinetic, chronoamperometry, and X-ray crystallographic data (PDF, CIF). This material is available free of charge via the Internet at <http://pubs.acs.org>.

JA054167+